

Properties of heavy quarkonia and B_c mesons in the relativistic quark model

D. Ebert

*Institut für Physik, Humboldt-Universität zu Berlin,
Invalidenstrasse 110, D-10115 Berlin, Germany*

R. N. Faustov and V. O. Galkin

*Institut für Physik, Humboldt-Universität zu Berlin,
Invalidenstrasse 110, D-10115 Berlin, Germany and*

*Russian Academy of Sciences, Scientific Council for Cybernetics,
Vavilov Street 40, Moscow 117333, Russia*

The mass spectra and electromagnetic decay rates of charmonium, bottomonium and B_c mesons are comprehensively investigated in the relativistic quark model. The presence of only heavy quarks allows the expansion in powers of their velocities. All relativistic corrections of order v^2/c^2 , including retardation effects and one-loop radiative corrections, are systematically taken into account in the computations of the mass spectra. The obtained wave functions are used for the calculation of radiative magnetic dipole (M1) and electric dipole (E1) transitions. It is found that relativistic effects play a substantial role. Their account and the proper choice of the Lorentz structure of the quark-antiquark interaction in a meson is crucial for bringing theoretical predictions in accord with experimental data. A detailed comparison of the calculated decay rates and branching fractions with available experimental data for radiative decays of charmonium and bottomonium is presented. The possibilities to observe the currently missing spin-singlet S and P states as well as D states in bottomonium are discussed. The results for B_c masses and decays are compared with other quark model predictions.

PACS numbers: 12.40.Yx, 12.39.Ki, 13.40.Hq, 14.40.Gx

I. INTRODUCTION

The investigation of the properties of mesons composed of a heavy quark and antiquark ($b\bar{b}$, $c\bar{c}$, $c\bar{b}$) gives very important insight into heavy quark dynamics. Heavy quarkonia have a rich spectroscopy with many narrow states lying under the threshold of open flavour production. Excited states experience different decays among which there are radiative transitions to lower levels. The theoretical analysis shows that many properties of heavy quarkonia, including mass spectra and radiative decay rates, are significantly influenced by relativistic effects. Thus their inclusion is necessary for the correct description of the spectroscopy and the determination of quarkonium wave functions. Radiative decays are the most sensitive to relativistic effects. Some of these decays, which are forbidden in the

exact nonrelativistic limit (so-called hindered transitions) due to the orthogonality of initial and final meson wave functions, have decay rates of the same order as the allowed ones. In the relativistic description of mesons an important role is played by properties of the confining quark-antiquark interaction, in particular its Lorentz structure. Thus comparison of theoretical predictions with experimental data can provide valuable information on the form of the confining potential. Such information is of great practical interest, since at present it is not possible to obtain the $Q\bar{Q}$ potential in the whole range of distances from the basic principles of quantum chromodynamics (QCD). As it is well known, the growing of the strong coupling constant with distance makes perturbation theory inapplicable at large distances (in the infrared region). In this region it is necessary to account for nonperturbative effects connected with the complicated structure of the QCD vacuum. All this leads to a theoretical uncertainty in the $Q\bar{Q}$ potential at large and intermediate distances. It is just in this region of large and intermediate distances that most of the basic meson characteristics are formed.

At present, a vast set of experimental data is available on the masses and different decays of heavy quarkonia. However, not all states predicted by theory have been observed yet, while the others need confirmation. Such missing or unconfirmed states are present both in charmonium (2^1S_0 , 1^1P_1 , 1^1D_2 , $1^3D_{2,3}$) and bottomonium (spin-singlet 1S_0 and 1P_1 states, D states). The different possibilities for their experimental observation are proposed and widely discussed in the literature [1, 2, 3, 4, 5, 6]. Radiative transitions from the spin-triplet levels with $J^{PC} = 1^{--}$ to these states as well as their subsequent radiative decays play an important role in these proposals. The missing charmonium states can also be searched in B meson decays and identified by their radiative transitions [1, 2]. For this purpose, reliable relativistic predictions for the masses of these states and for the rates of radiative transitions involving them are necessary.

The properties of the B_c meson are of special interest, since it is the only heavy meson consisting of two heavy quarks with different flavour. This difference of quark flavours forbids annihilation into gluons. As a result, the excited B_c meson states lying below the BD production threshold undergo pionic or radiative transitions to the ground pseudoscalar state which then decays weakly. There should be a rather rich set of such narrow states which are considerably more stable than corresponding charmonium or bottomonium states. The CDF collaboration [7] reported the discovery of the B_c ground state in $p\bar{p}$ collisions at Fermilab. More experimental data are expected to come in the near future from new hadronic colliders.

The purpose of this paper is to give a detailed analysis of mass spectra and radiative transitions in charmonium, bottomonium and B_c mesons with the comprehensive account of the relativistic effects. This will allow one to get valuable information about the Lorentz structure of confining quark interactions from the comparison of obtained predictions with available experimental data. On the other hand, it will indicate the processes in which the missing states can be searched for.

The paper is organized as follows. In Sec. II we describe our relativistic quark model. The expression for the heavy quark-antiquark quasipotential with the account of relativistic (including retardation effects) and one loop radiative corrections is given in Sec. III. There it is applied to the calculation of the charmonium, bottomonium and B_c meson mass spectra. In Sec. IV pseudoscalar and vector decay constants of the B_c meson are calculated with the account of relativistic corrections and compared with other theoretical predictions. In Sec. V the relativistic expressions for the radiative transition matrix elements in the quasipotential

approach are given. They are used for the calculation of the decay rates of radiative M1 and E1 transitions in Secs. VI and VII, respectively. The role of relativistic effects in these transitions is investigated. Special attention is paid to the influence of the Lorentz structure of the quark potential on the relativistic corrections to decay rates. Pure vector and scalar potentials as well as their mixture are considered. The obtained results are compared with available experimental data, and the possibilities for searching the missing states in bottomonium are discussed. Finally, our conclusions are given in Sec. VIII.

II. RELATIVISTIC QUARK MODEL

In the quasipotential approach a meson is described by the wave function of the bound quark-antiquark state, which satisfies the quasipotential equation [8] of the Schrödinger type [9]

$$\left(\frac{b^2(M)}{2\mu_R} - \frac{\mathbf{p}^2}{2\mu_R} \right) \Psi_M(\mathbf{p}) = \int \frac{d^3q}{(2\pi)^3} V(\mathbf{p}, \mathbf{q}; M) \Psi_M(\mathbf{q}), \quad (1)$$

where the relativistic reduced mass is

$$\mu_R = \frac{E_1 E_2}{E_1 + E_2} = \frac{M^4 - (m_1^2 - m_2^2)^2}{4M^3}, \quad (2)$$

and E_1, E_2 are given by

$$E_1 = \frac{M^2 - m_2^2 + m_1^2}{2M}, \quad E_2 = \frac{M^2 - m_1^2 + m_2^2}{2M}. \quad (3)$$

Here $M = E_1 + E_2$ is the meson mass, $m_{1,2}$ are the quark masses, and \mathbf{p} is their relative momentum. In the center of mass system the relative momentum squared on mass shell reads

$$b^2(M) = \frac{[M^2 - (m_1 + m_2)^2][M^2 - (m_1 - m_2)^2]}{4M^2}. \quad (4)$$

The kernel $V(\mathbf{p}, \mathbf{q}; M)$ in Eq. (1) is the quasipotential operator of the quark-antiquark interaction. It is constructed with the help of the off-mass-shell scattering amplitude, projected onto the positive energy states. Constructing the quasipotential of the quark-antiquark interaction, we have assumed that the effective interaction is the sum of the usual one-gluon exchange term with the mixture of long-range vector and scalar linear confining potentials, where the vector confining potential contains the Pauli interaction. The quasipotential is then defined by [10]

$$V(\mathbf{p}, \mathbf{q}; M) = \bar{u}_1(p) \bar{u}_2(-p) \mathcal{V}(\mathbf{p}, \mathbf{q}; M) u_1(q) u_2(-q), \quad (5)$$

with

$$\mathcal{V}(\mathbf{p}, \mathbf{q}; M) = \frac{4}{3} \alpha_s D_{\mu\nu}(\mathbf{k}) \gamma_1^\mu \gamma_2^\nu + V_{\text{conf}}^V(\mathbf{k}) \Gamma_1^\mu \Gamma_{2;\mu} + V_{\text{conf}}^S(\mathbf{k}),$$

where α_s is the QCD coupling constant, $D_{\mu\nu}$ is the gluon propagator in the Coulomb gauge

$$D^{00}(\mathbf{k}) = -\frac{4\pi}{\mathbf{k}^2}, \quad D^{ij}(\mathbf{k}) = -\frac{4\pi}{k^2} \left(\delta^{ij} - \frac{k^i k^j}{\mathbf{k}^2} \right), \quad D^{0i} = D^{i0} = 0, \quad (6)$$

and $\mathbf{k} = \mathbf{p} - \mathbf{q}$; γ_μ and $u(p)$ are the Dirac matrices and spinors

$$u^\lambda(p) = \sqrt{\frac{\epsilon(p) + m}{2\epsilon(p)}} \begin{pmatrix} 1 \\ \frac{\boldsymbol{\sigma}\mathbf{p}}{\epsilon(p) + m} \end{pmatrix} \chi^\lambda, \quad (7)$$

with $\epsilon(p) = \sqrt{p^2 + m^2}$. The effective long-range vector vertex is given by

$$\Gamma_\mu(\mathbf{k}) = \gamma_\mu + \frac{i\kappa}{2m} \sigma_{\mu\nu} k^\nu, \quad (8)$$

where κ is the Pauli interaction constant characterizing the anomalous chromomagnetic moment of quarks. Vector and scalar confining potentials in the nonrelativistic limit reduce to

$$\begin{aligned} V_V(r) &= (1 - \varepsilon)Ar + B, \\ V_S(r) &= \varepsilon Ar, \end{aligned} \quad (9)$$

reproducing

$$V_{\text{conf}}(r) = V_S(r) + V_V(r) = Ar + B, \quad (10)$$

where ε is the mixing coefficient.

The expression for the quasipotential of the heavy quarkonia, expanded in v^2/c^2 without and with retardation corrections to the confining potential, can be found in Refs. [10] and [11], respectively. The structure of the spin-dependent interaction is in agreement with the parameterization of Eichten and Feinberg [12]. The quasipotential for the heavy quark interaction with light antiquark without employing the expansion in inverse powers of the light quark mass is given in Ref. [13]. All the parameters of our model such as quark masses, parameters of the linear confining potential A and B , mixing coefficient ε and anomalous chromomagnetic quark moment κ are fixed from the analysis of heavy quarkonium masses [11] (see Sec. III) and radiative decays [14] (see Secs. V–VII). The quark masses $m_b = 4.88$ GeV, $m_c = 1.55$ GeV and the parameters of the linear potential $A = 0.18$ GeV² and $B = -0.16$ GeV have usual values of quark models. The value of the mixing coefficient of vector and scalar confining potentials $\varepsilon = -1$ has been determined from the consideration of the heavy quark expansion for the semileptonic $B \rightarrow D$ decays [15] and charmonium radiative decays [14]. Finally, the universal Pauli interaction constant $\kappa = -1$ has been fixed from the analysis of the fine splitting of heavy quarkonia 3P_J - states [10]. Note that the long-range magnetic contribution to the potential in our model is proportional to $(1 + \kappa)$ and thus vanishes for the chosen value of $\kappa = -1$. In the present paper we will take into consideration the retardation corrections as well as one-loop radiative corrections.

III. HEAVY QUARKONIUM AND B_c MESON MASS SPECTRA

The heavy quark-antiquark potential with the account of retardation effects and one loop radiative corrections can be presented in the form of a sum of spin-independent and spin-dependent parts. For the spin-independent part we have [11]

$$V_{\text{SI}}(r) = -\frac{4}{3} \frac{\bar{\alpha}_V(\mu^2)}{r} + Ar + B - \frac{4}{3} \frac{\beta_0 \alpha_s^2(\mu^2)}{2\pi} \frac{\ln(\mu r)}{r}$$

$$\begin{aligned}
& + \frac{1}{8} \left(\frac{1}{m_1^2} + \frac{1}{m_2^2} \right) \Delta \left[-\frac{4 \bar{\alpha}_V(\mu^2)}{3 r} - \frac{4 \beta_0 \alpha_s^2(\mu^2) \ln(\mu r)}{3 \cdot 2\pi r} + (1 - \varepsilon)(1 + 2\kappa)Ar \right] \\
& + \frac{1}{2m_1 m_2} \left(\left\{ -\frac{4 \bar{\alpha}_V}{3 r} \left[\mathbf{p}^2 + \frac{(\mathbf{p} \cdot \mathbf{r})^2}{r^2} \right] \right\}_W \right. \\
& \left. - \frac{4 \beta_0 \alpha_s^2(\mu^2)}{3 \cdot 2\pi} \left\{ \mathbf{p}^2 \frac{\ln(\mu r)}{r} + \frac{(\mathbf{p} \cdot \mathbf{r})^2}{r^2} \left(\frac{\ln(\mu r)}{r} - \frac{1}{r} \right) \right\}_W \right) \\
& + \left[\frac{1 - \varepsilon}{2m_1 m_2} - \frac{\varepsilon}{4} \left(\frac{1}{m_1^2} + \frac{1}{m_2^2} \right) \right] \left\{ Ar \left[\mathbf{p}^2 - \frac{(\mathbf{p} \cdot \mathbf{r})^2}{r^2} \right] \right\}_W \\
& + \left[\frac{1}{4} \left(\frac{1}{m_1^2} + \frac{1}{m_2^2} \right) + \frac{1}{m_1 m_2} \right] B \mathbf{p}^2, \tag{11}
\end{aligned}$$

where

$$\begin{aligned}
\bar{\alpha}_V(\mu^2) &= \alpha_s(\mu^2) \left[1 + \left(\frac{a_1}{4} + \frac{\gamma_E \beta_0}{2} \right) \frac{\alpha_s(\mu^2)}{\pi} \right], \tag{12} \\
a_1 &= \frac{31}{3} - \frac{10}{9} n_f, \\
\beta_0 &= 11 - \frac{2}{3} n_f.
\end{aligned}$$

Here n_f is the number of flavours and μ is a renormalization scale. Note that for a quantity quadratic in the momenta we use the Weyl prescription [16]:

$$\{f(r)p^i p^j\}_W = \frac{1}{4} \{ \{f(r), p^i\}, p^j \}.$$

For the dependence of the QCD coupling constant $\alpha_s(\mu^2)$ on the renormalization point μ^2 we use the leading order result

$$\alpha_s(\mu^2) = \frac{4\pi}{\beta_0 \ln(\mu^2/\Lambda^2)}. \tag{13}$$

In our numerical calculations we set the renormalization scale $\mu = 2m_1 m_2 / (m_1 + m_2)$ and $\Lambda = 0.168$ GeV, which gives $\alpha_s = 0.314$ for $m_1 = m_2 = m_c$ (charmonium); $\alpha_s = 0.223$ for $m_1 = m_2 = m_b$ (bottomonium); and $\alpha_s = 0.265$ for $m_1 = m_c, m_2 = m_b$ (B_c meson).

The spin-dependent part of the quark-antiquark potential for unequal quark masses with the inclusion of radiative corrections [17, 18] can be presented in our model as follows:

$$V_{SD}(r) = a \mathbf{L} \cdot \mathbf{S} + b \left[\frac{3}{r^2} (\mathbf{S}_1 \cdot \mathbf{r})(\mathbf{S}_2 \cdot \mathbf{r}) - (\mathbf{S}_1 \cdot \mathbf{S}_2) \right] + c \mathbf{S}_1 \cdot \mathbf{S}_2 + d \mathbf{L} \cdot (\mathbf{S}_1 - \mathbf{S}_2), \tag{14}$$

$$\begin{aligned}
a &= \frac{1}{4} \left(\frac{1}{m_1^2} + \frac{1}{m_2^2} \right) \left\{ \frac{4 \alpha_s(\mu^2)}{3 r^3} \left(1 + \frac{\alpha_s(\mu^2)}{\pi} \left[\frac{7}{3} - \frac{\beta_0}{12} + \gamma_E \left(\frac{\beta_0}{2} - 3 \right) + \frac{\beta_0}{2} \ln(\mu r) \right. \right. \right. \\
& \left. \left. \left. - 3 \ln(\sqrt{m_1 m_2} r) \right) \right] - \frac{A}{r} \right\} + \frac{1}{m_1 m_2} \frac{4 \alpha_s(\mu^2)}{3 r^3} \left(1 + \frac{\alpha_s(\mu^2)}{\pi} \left[\frac{1}{6} - \frac{\beta_0}{12} \right. \right. \right.
\end{aligned}$$

$$\begin{aligned}
& +\gamma_E \left(\frac{\beta_0}{2} - \frac{3}{2} \right) + \frac{\beta_0}{2} \ln(\mu r) - \frac{3}{2} \ln(\sqrt{m_1 m_2} r) \Big] \Big) \\
& + \left(\frac{1}{m_1^2} - \frac{1}{m_2^2} \right) \frac{\alpha_s^2(\mu^2)}{2\pi r^3} \ln \frac{m_2}{m_1} + \frac{1}{2} \left(\frac{1}{m_1} + \frac{1}{m_2} \right)^2 (1 + \kappa)(1 - \varepsilon) \frac{A}{r}, \tag{15}
\end{aligned}$$

$$\begin{aligned}
b = \frac{1}{3m_1 m_2} \Big\{ & \frac{4\alpha_s(\mu^2)}{r^3} \left(1 + \frac{\alpha_s(\mu^2)}{\pi} \left[\frac{29}{6} - \frac{1}{4}\beta_0 + \gamma_E \left(\frac{\beta_0}{2} - 3 \right) + \frac{\beta_0}{2} \ln(\mu r), \right. \right. \\
& \left. \left. - 3 \ln(\sqrt{m_1 m_2} r) \right] \right) + (1 + \kappa)^2 (1 - \varepsilon) \frac{A}{r} \Big\}, \tag{16}
\end{aligned}$$

$$\begin{aligned}
c = \frac{4}{3m_1 m_2} \Big\{ & \frac{8\pi\alpha_s(\mu^2)}{3} \left(\left[1 + \frac{\alpha_s(\mu^2)}{\pi} \left(\frac{5}{12}\beta_0 - \frac{11}{3} - \left[\frac{m_1 - m_2}{m_1 + m_2} + \frac{1}{8} \frac{m_1 + m_2}{m_1 - m_2} \right] \ln \frac{m_2}{m_1} \right) \right] \delta^3(r) \right. \\
& + \frac{\alpha_s(\mu^2)}{\pi} \left[-\frac{\beta_0}{8\pi} \nabla^2 \left(\frac{\ln(\mu r) + \gamma_E}{r} \right) + \frac{21}{16\pi} \nabla^2 \left(\frac{\ln(\sqrt{m_1 m_2} r) + \gamma_E}{r} \right) \right] \Big) \\
& \left. + (1 + \kappa)^2 (1 - \varepsilon) \frac{A}{r} \right\}, \tag{17}
\end{aligned}$$

$$\begin{aligned}
d = \frac{1}{4} \left(\frac{1}{m_1^2} - \frac{1}{m_2^2} \right) \Big\{ & \frac{4}{3} \frac{\alpha_s(\mu^2)}{r^3} \left(1 + \frac{\alpha_s(\mu^2)}{\pi} \left[\frac{7}{3} - \frac{\beta_0}{12} + \gamma_E \left(\frac{\beta_0}{2} - 3 \right) + \frac{\beta_0}{2} \ln(\mu r) \right. \right. \\
& \left. \left. - 3 \ln(\sqrt{m_1 m_2} r) \right] \right) - \frac{A}{r} - 2(1 + \kappa)(1 - \varepsilon) \frac{A}{r} \Big\} + \left(\frac{1}{m_1} + \frac{1}{m_2} \right)^2 \frac{\alpha_s^2(\mu^2)}{2\pi r^3} \ln \frac{m_2}{m_1}, \tag{18}
\end{aligned}$$

where \mathbf{L} is the orbital momentum and $\mathbf{S}_{1,2}$, $\mathbf{S} = \mathbf{S}_1 + \mathbf{S}_2$ are the spin momenta. For the equal mass case ($m_1 = m_2 = m$) the second order in α_s contribution of the annihilation diagrams

$$\delta c = \frac{8\alpha_s^2(\mu^2)}{3m^2} (1 - \ln 2) \delta^3(r) \tag{19}$$

must be added to the spin-spin interaction coefficient c in Eq. (17).

The correct description of the fine structure of the heavy quarkonium mass spectrum requires the vanishing of the vector confinement contribution. This can be achieved by setting $1 + \kappa = 0$, i.e., the total long-range quark chromomagnetic moment equals zero, which is in accord with the flux tube [19] and minimal area [16, 20] models. One can see from Eq. (14) that for the spin-dependent part of the potential this conjecture is equivalent to the assumption about the scalar structure of confining interaction [21].

To calculate the heavy meson mass spectra with the account of all relativistic corrections (including retardation effects) of order v^2/c^2 and one-loop radiative corrections we substitute the quasipotential which is a sum of the spin-independent (11) and spin-dependent (14) parts into the quasipotential equation (1). Then we multiply the resulting expression from the left by the quasipotential wave function of a bound state and integrate with respect to the relative momentum. Taking into account the accuracy of the calculations, we can use for

the resulting matrix elements the wave functions of Eq. (1) with the static potential ¹

$$V_{\text{NR}}(r) = -\frac{4\bar{\alpha}_V(\mu^2)}{3} \frac{1}{r} + Ar + B. \quad (20)$$

As a result we obtain the mass formula

$$\frac{b^2(M)}{2\mu_R} = W + \langle a \rangle \langle \mathbf{L} \cdot \mathbf{S} \rangle + \langle b \rangle \left\langle \left[\frac{3}{r^2} (\mathbf{S}_1 \cdot \mathbf{r})(\mathbf{S}_2 \cdot \mathbf{r}) - (\mathbf{S}_1 \cdot \mathbf{S}_2) \right] \right\rangle + \langle c \rangle \langle \mathbf{S}_1 \cdot \mathbf{S}_2 \rangle + d \langle \mathbf{L} \cdot (\mathbf{S}_1 - \mathbf{S}_2) \rangle, \quad (21)$$

where

$$W = \langle V_{\text{SI}} \rangle + \frac{\langle \mathbf{p}^2 \rangle}{2\mu_R}. \quad (22)$$

The first term on the right-hand side of the mass formula (21) contains all spin-independent contributions, the second and the last terms describe the spin-orbit interaction, the third term is responsible for the tensor interaction, while the fourth term gives the spin-spin interaction. The last term is not zero only for the unequal mass case $m_1 \neq m_2$ and leads to the mixing of triplet and singlet meson states with the total angular momentum J equal to the orbital momentum L .

In Table I the calculated charmonium mass spectrum is compared with experimental data. For meson states we use the notation $n^{2S+1}L_J$, where $n = n_r + 1$ and n_r is the radial quantum number. Our predictions agree with PDG [22] data within a few MeV. Our model correctly reproduces both the position of the levels and their fine and hyperfine splittings. In this Table we also give the recent Belle Collaboration data [23] on pseudoscalar $\eta_c(1^1S_0)$ and $\eta'_c(2^1S_0)$ states observed in B decays. The measured mass of the ground spin-singlet state $\eta_c(1^1S_0)$ is in good agreement with world averages and predictions of our model, while the radially excited $\eta'_c(2^1S_0)$ state lies considerably higher than previous experimental indications and most of the theoretical predictions. If these data are confirmed, it will be difficult to accommodate such a small hyperfine splitting ≈ 32 MeV (almost four times smaller than 117 MeV splitting for the ground state) in the framework of the quark model. ²

Our prediction for the mass of $h_c(1^1P_1)$ is consistent with the data from the Fermilab Experiment E760 [25] on $p\bar{p} \rightarrow h_c(3526) \rightarrow \pi^0 J/\Psi$ which, however, need confirmation. The same is true for the indication of a 1^3D_2 state with mass 3836 ± 13 MeV in $\pi^\pm N \rightarrow J/\Psi \pi^+ \pi^- + \text{anything}$ [26].

For the calculation of the bottomonium mass spectrum it is also necessary to take into account additional one-loop corrections due to the finite mass of the charm quark [27, 28, 29, 30]. We considered these corrections within our model in Ref. [31] and found that they give contributions of a few MeV and are weakly dependent on the quantum numbers of the bottomonium states. The one-loop correction to the static $Q\bar{Q}$ potential in QCD due to the finite c quark mass is given by [29, 31]

$$\Delta V(r, m_c) = -\frac{4\alpha_s^2(\mu)}{9\pi r} [\ln(\sqrt{a_0}m_c r) + \gamma_E + E_1(\sqrt{a_0}m_c r)], \quad (23)$$

¹ This static potential includes also some radiative corrections. The remaining radiative correction term with logarithm in Eq. (11), also not vanishing in the static limit, is treated perturbatively.

² The position of the $\Psi'(2^3S_1)$ can in principle be influenced by the nearby threshold of the open charm production.

TABLE I: Charmonium mass spectrum (in GeV).

State $n^{2S+1}L_J$	Particle	Theory	Experiment	
			PDG [22]	Belle [23]
1^1S_0	η_c	2.979	2.9797	2.979
1^3S_1	J/Ψ	3.096	3.09687	
1^3P_0	χ_{c0}	3.424	3.4151	
1^3P_1	χ_{c1}	3.510	3.51051	
1^3P_2	χ_{c2}	3.556	3.55618	
1^1P_1	h_c	3.526		
2^1S_0	η'_c	3.588	3.594 ^a	3.654
2^3S_1	Ψ'	3.686	3.68596	
1^3D_1		3.798	3.7699 ^b	
1^3D_2		3.813		
1^3D_3		3.815		
1^1D_2		3.811		
2^3P_0	χ'_{c0}	3.854		
2^3P_1	χ'_{c1}	3.929		
2^3P_2	χ'_{c2}	3.972		
2^1P_1	h'_c	3.945		
3^1S_0	η''_c	3.991		
3^3S_1	Ψ''	4.088	4.040 ^b	

^aThis value from Ref. [24] is included only in the PDG Listings.

^b Mixture of S and D states.

where

$$E_1(x) = \int_x^\infty e^{-t} \frac{dt}{t} = -\gamma_E - \ln x - \sum_{n=1}^{\infty} \frac{(-x)^n}{n \cdot n!},$$

$\gamma_E \cong 0.5772$ is the Euler constant and $a_0 = 5.2$. The resulting bottomonium mass spectrum with the account of this correction is given in Table II. We found that the small shift of the QCD parameter Λ from our previous [11] value 0.178 to 0.168 GeV (with all other parameters remaining fixed) allows us to get a good fit to the bottomonium mass spectrum with the account of finite charm quark mass corrections. The difference between the theoretical and experimental data is less than 3 MeV. Very recently CLEO Collaboration presented [32] the first evidence for the production of the triplet $\Upsilon(1D)$ state in the four photon cascades starting from $\Upsilon(3S)$. In Table II we give their preliminary result for the mass of $\Upsilon(1D_2)$ state which is consistent with our prediction.

For the mesons consisting of quarks with different flavours ($m_1 \neq m_2$), such as the B_c meson, the coefficient d (18) in the spin-dependent part of the quark potential (14) is not equal to zero. This results in the mixing of singlet and triplet P states with $J = 1$,

$$\begin{aligned} nP1' &= n^1P_1 \cos \theta_{nP} + n^3P_1 \sin \theta_{nP}, \\ nP1 &= -n^1P_1 \sin \theta_{nP} + n^3P_1 \cos \theta_{nP}, \end{aligned} \tag{24}$$

TABLE II: Bottomonium mass spectrum (in GeV).

State $n^{2S+1}L_J$	Particle	Theory	Experiment	
			PDG [22]	CLEO [32]
1^1S_0	η_b	9.400		
1^3S_1	Υ	9.460	9.46030	
1^3P_0	χ_{b0}	9.863	9.8599	
1^3P_1	χ_{b1}	9.892	9.8927	
1^3P_2	χ_{b2}	9.913	9.9126	
1^1P_1	h_b	9.901		
2^1S_0	η'_b	9.993		
2^3S_1	Υ'	10.023	10.02326	
1^3D_1		10.153		
1^3D_2		10.158		10.162
1^3D_3		10.162		
1^1D_2		10.158		
2^3P_0	χ'_{b0}	10.234	10.2321	
2^3P_1	χ'_{b1}	10.255	10.2552	10.2556
2^3P_2	χ'_{b2}	10.268	10.2685	10.2688
2^1P_1	h'_b	10.261		
3^1S_0	η''_b	10.328		
3^3S_1	Υ''	10.355	10.3552	

and of D states with $J = 2$,

$$\begin{aligned}
 nD2' &= n^1D_2 \cos \theta_{nD} + n^3D_2 \sin \theta_{nD}, \\
 nD2 &= -n^1D_2 \sin \theta_{nD} + n^3D_2 \cos \theta_{nD}.
 \end{aligned}
 \tag{25}$$

For the B_c meson the values of the mixing angles in our model are

$$\theta_{1P} = 0.357, \quad \theta_{2P} = 0.405, \quad \theta_{1D} = -0.627.
 \tag{26}$$

In Table III we compare our model predictions for the mass spectrum of the B_c meson with other quark model results [33, 34, 35, 36]. We see that the differences between the predictions in most cases do not exceed 30 MeV. The only exceptions are masses of $1D$ states, which are 50 – 70 MeV heavier in our model. The fine and hyperfine splittings are also consistent with each other. All these predictions for the ground state pseudoscalar B_c and vector B_c^* meson masses satisfy the bounds found by Kwong and Rosner [37]:

$$6.194 \text{ GeV} < M_{B_c} < 6.292 \text{ GeV}$$

and

$$6.284 \text{ GeV} < M_{B_c^*} < 6.357 \text{ GeV}.$$

In Ref. [38] the ground state B_c mass was evaluated in perturbative QCD. Experimental data [22] at present are available only for the B_c ground state and have large error bars $M_{B_c} = 6.4 \pm 0.4 \text{ GeV}$.

TABLE III: B_c meson mass spectrum (in GeV).

State $n^{2S+1}L_J$	Our	[33]	[34]	[35]	[36]
1^1S_0	6.270	6.264	6.253	6.286	≥ 6.2196
1^3S_1	6.332	6.337	6.317	6.341	≥ 6.2786
1^3P_0	6.699	6.700	6.683	6.701	≥ 6.6386
$1P1$	6.734	6.730	6.717	6.737	≥ 6.7012
$1P1'$	6.749	6.736	6.729	6.760	≥ 6.7012
1^3P_2	6.762	6.747	6.743	6.772	≥ 6.7347
2^1S_0	6.835	6.856	6.867	6.882	
2^3S_1	6.881	6.899	6.902	6.914	
1^3D_1	7.072	7.012	7.008	7.019	
$1D2$	7.077	7.009	7.001	7.028	
$1D2'$	7.079	7.012	7.016	7.028	
1^3D_3	7.081	7.005	7.007	7.032	
2^3P_0	7.091	7.108	7.088		
$2P1$	7.126	7.135	7.113		
$2P1'$	7.145	7.142	7.124		
2^3P_2	7.156	7.153	7.134		
3^1S_0	7.193	7.244			
3^3S_1	7.235	7.280			

In the following sections we apply the masses and wave functions of Ψ , Υ and B_c mesons for the calculation of their decay constants and decay rates.

IV. PSEUDOSCALAR AND VECTOR DECAY CONSTANTS OF THE B_c MESON

The B_c meson and its first excitations which lie below the BD threshold are stable against strong decays, since they cannot annihilate into gluons. They can decay via electromagnetic and pionic transitions into the lightest pseudoscalar ground state B_c . The significant contribution to the B_c total decay rate comes from the annihilation of the c quark and \bar{b} antiquark into the vector boson W^+ which decays into a lepton and a neutrino or a quark-antiquark pair. The weak annihilation decay rate is determined by the pseudoscalar constant of the B_c meson.

The decay constants f_P and f_V of the pseudoscalar (P) and vector (V) mesons parameterize the matrix elements of the weak current between the corresponding meson and the vacuum. In the case of the B_c meson they are defined by

$$\langle 0 | \bar{b} \gamma^\mu \gamma_5 c | P(\mathbf{K}) \rangle = i f_P K^\mu, \quad (27)$$

$$\langle 0 | \bar{b} \gamma^\mu c | V(\mathbf{K}, \varepsilon) \rangle = f_V M_V \varepsilon^\mu, \quad (28)$$

where \mathbf{K} is the meson momentum, P corresponds to the pseudoscalar B_c and V to the vector

B_c^* mesons, ε^μ and M_V are the polarisation vector and mass of the vector B_c^* meson.

In the relativistic quark model the decay constants can be expressed through the meson wave function $\Phi_{P,V}(p)$ in the momentum space and are given by [39]

$$f_{P,V} = \sqrt{\frac{12}{M_{P,V}}} \int \frac{d^3p}{(2\pi)^3} \left(\frac{\epsilon_c(p) + m_c}{2\epsilon_c(p)} \right)^{1/2} \left(\frac{\epsilon_b(p) + m_b}{2\epsilon_b(p)} \right)^{1/2} \times \left\{ 1 + \lambda_{P,V} \frac{\mathbf{p}^2}{[\epsilon_c(p) + m_c][\epsilon_b(p) + m_b]} \right\} \Phi_{P,V}(p), \quad (29)$$

with $\lambda_P = -1$ and $\lambda_V = 1/3$. In the nonrelativistic limit $p^2/m^2 \rightarrow 0$ these expressions for decay constants give the well-known formula

$$f_P^{\text{NR}} = f_V^{\text{NR}} = \sqrt{\frac{12}{M_{P,V}}} |\Psi_{P,V}(0)|, \quad (30)$$

where $\Psi_{P,V}(0)$ is the meson wave function at the origin $r = 0$.

The calculated values of the pseudoscalar and vector decay constants of the B_c meson in our model using the relativistic formula (29) are displayed in Table IV. They are compared with the ones calculated using the nonrelativistic expression (30) and other predictions of the nonrelativistic quark models [33, 35], QCD sum rules [34] and lattice NRQCD [40]. We see that inclusion of relativistic corrections reduces the pseudoscalar decay constant f_{B_c} by 20% and produces the difference between vector and pseudoscalar decay constants of approximately 70 MeV. The calculated values of these decay constants are consistent with lattice [40] and QCD sum rule [34] predictions.

TABLE IV: Pseudoscalar and vector decay constants ($f_P = f_{B_c}$, $f_V = f_{B_c^*}$) of the B_c meson (in MeV).

Constant	rel	NR	[33]	[34]	[35]	[40]
f_{B_c}	433	562	500	460 ± 60	517	420 ± 13
$f_{B_c^*}$	503	562	500	460 ± 60	517	

V. RADIATIVE TRANSITIONS IN HEAVY QUARKONIA AND B_c MESONS

To determine the rates of radiative decays ($B \rightarrow A + \gamma$) it is necessary to calculate the matrix element of the electromagnetic current J_μ between the initial (B) and final (A) meson states. In the quasipotential approach such matrix element has the form [41]

$$\langle A | J_\mu(0) | B \rangle = \int \frac{d^3p d^3q}{(2\pi)^6} \bar{\Psi}_{A\mathbf{P}}(\mathbf{p}) \Gamma_\mu(\mathbf{p}, \mathbf{q}) \Psi_{B\mathbf{Q}}(\mathbf{q}), \quad (31)$$

where $\Gamma_\mu(\mathbf{p}, \mathbf{q})$ is the two-particle vertex function and $\Psi_{A,B}$ are the meson wave functions projected onto the positive energy states of quarks and boosted to the moving reference frame. The contributions to Γ come from Figs. 1 and 2. The contribution $\Gamma^{(2)}$ is the consequence of the projection onto the positive-energy states. Note that the form of the

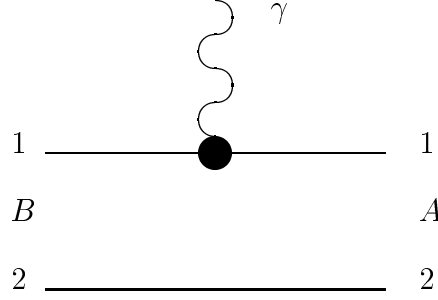


FIG. 1: Lowest order vertex function $\Gamma^{(1)}$ corresponding to Eq. (33). Radiation only from one quark is shown.

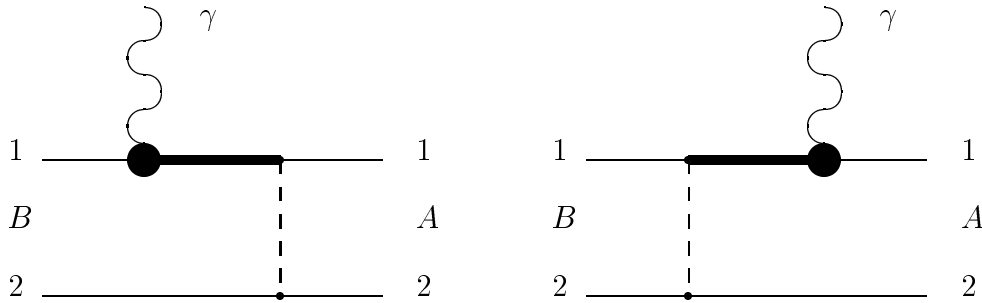


FIG. 2: Vertex function $\Gamma^{(2)}$ corresponding to Eq. (34). Dashed lines represent the interaction operator \mathcal{V} in Eq. (5). Bold lines denote the negative-energy part of the quark propagator. As on Fig. 1, radiation only from one quark is shown.

relativistic corrections resulting from the vertex function $\Gamma^{(2)}$ explicitly depends on the Lorentz structure of the $Q\bar{Q}$ -interaction. Thus the vertex function is given by

$$\Gamma_\mu(\mathbf{p}, \mathbf{q}) = \Gamma_\mu^{(1)}(\mathbf{p}, \mathbf{q}) + \Gamma_\mu^{(2)}(\mathbf{p}, \mathbf{q}) + \dots, \quad (32)$$

where

$$\Gamma_\mu^{(1)}(\mathbf{p}, \mathbf{q}) = e_1 \bar{u}_1(p_1) \gamma_\mu u_1(q_1) (2\pi)^3 \delta(\mathbf{p}_2 - \mathbf{q}_2) + (1 \leftrightarrow 2), \quad (33)$$

and

$$\begin{aligned} \Gamma_\mu^{(2)}(\mathbf{p}, \mathbf{q}) = e_1 \bar{u}_1(p_1) \bar{u}_2(p_2) \left\{ \mathcal{V}(\mathbf{p}_2 - \mathbf{q}_2) \frac{\Lambda_1^{(-)}(k'_1)}{\epsilon_1(k'_1) + \epsilon_1(q_1)} \gamma_1^0 \gamma_{1\mu} \right. \\ \left. + \gamma_{1\mu} \frac{\Lambda_1^{(-)}(k_1)}{\epsilon_1(k_1) + \epsilon_1(p_1)} \gamma_1^0 \mathcal{V}(\mathbf{p}_2 - \mathbf{q}_2) \right\} u_1(q_1) u_2(q_2) + (1 \leftrightarrow 2). \end{aligned} \quad (34)$$

Here $e_{1,2}$ are the quark charges, $\mathbf{k}_1 = \mathbf{p}_1 - \mathbf{\Delta}$; $\mathbf{k}'_1 = \mathbf{q}_1 + \mathbf{\Delta}$; $\mathbf{\Delta} = \mathbf{P} - \mathbf{Q}$;

$$\Lambda^{(-)}(p) = \frac{\epsilon(p) - (m\gamma^0 + \gamma^0(\boldsymbol{\gamma} \cdot \mathbf{p}))}{2\epsilon(p)}, \quad \epsilon(p) = \sqrt{p^2 + m^2},$$

and

$$p_{1,2} = \epsilon_{1,2}(p) \frac{p_A}{M_A} \pm \sum_{i=1}^3 n^{(i)}(p_A) p^i,$$

$$q_{1,2} = \epsilon_{1,2}(q) \frac{p_B}{M_B} \pm \sum_{i=1}^3 n^{(i)}(p_B) q^i,$$

where $n^{(i)}$ are three four-vectors given by

$$n^{(i)\mu}(p) = \left\{ \frac{p^i}{M}, \delta_{ij} + \frac{p^i p^j}{M(E+M)} \right\}, \quad E = \sqrt{\mathbf{p}^2 + M^2}, \quad i, j = 1, 2, 3,$$

$p_B = (E_B, \mathbf{Q})$ and $p_A = (E_A, \mathbf{P})$ are four-momenta of initial and final mesons.

It is important to note that the wave functions entering the current matrix element (31) cannot be both in the rest frame. In the initial B meson rest frame, the final A meson is moving with the recoil momentum Δ . The wave function of the moving A meson $\Psi_{A\Delta}$ is connected with the wave function in the rest frame $\Psi_{A0} \equiv \Psi_A$ by the transformation [41]

$$\Psi_{A\Delta}(\mathbf{p}) = D_1^{1/2}(R_{L\Delta}^W) D_2^{1/2}(R_{L\Delta}^W) \Psi_{A0}(\mathbf{p}), \quad (35)$$

where R^W is the Wigner rotation, L_Δ is the Lorentz boost from the rest frame to a moving one, and the rotation matrix $D^{1/2}(R)$ in the spinor representation is given by

$$\begin{pmatrix} 1 & 0 \\ 0 & 1 \end{pmatrix} D_{1,2}^{1/2}(R_{L\Delta}^W) = S^{-1}(\mathbf{p}_{1,2}) S(\Delta) S(\mathbf{p}), \quad (36)$$

where

$$S(\mathbf{p}) = \sqrt{\frac{\epsilon(p) + m}{2m}} \left(1 + \frac{\boldsymbol{\alpha} \cdot \mathbf{p}}{\epsilon(p) + m} \right)$$

is the usual Lorentz transformation matrix of the four-spinor.

To calculate the radiative transition matrix element we adopt the following procedure. We substitute the vertex functions $\Gamma^{(1)}$ and $\Gamma^{(2)}$ given by Eqs. (33) and (34) in the decay matrix element (31) and take into account the wave function transformation (35). The resulting structure of this matrix element is rather complicated, because it is necessary to integrate both over d^3p and d^3q . The δ function in expression (33) permits us to perform one of these integrations and thus this contribution can be easily calculated. The calculation of the vertex function $\Gamma^{(2)}$ contribution is more difficult. Here, instead of a δ function, we have a complicated structure, containing the $Q\bar{Q}$ interaction potential in the meson. However, we can expand this contribution in powers of the heavy quark velocities v^2/c^2 and then use the quasipotential equation in order to perform one of the integrations in the current matrix element. It is easy to see that the vertex function $\Gamma^{(2)}$ contributes already at the first order of the v^2/c^2 expansion.

We consider two main types of radiative transitions:

- a) Magnetic dipole (M1) transitions which go with the spin flip of the quark ($\Delta S = 1$, $\Delta L = 0$) and thus the initial and final states belong to the same orbital excitation but have different spins. Examples of such transitions are vector to pseudoscalar ($n^3S_1 \rightarrow n'^1S_0 + \gamma$, $n \geq n'$) and pseudoscalar to vector ($n^1S_0 \rightarrow n'^3S_1 + \gamma$, $n > n'$) meson decays.
- b) Electric dipole (E1) transitions in which the orbital quantum number is changed ($\Delta L = 1$, $\Delta S = 0$) and thus the initial and final states belong to different orbital excitations but have the same spin. Examples of such transitions are $n^3S_1 \rightarrow n'^3P_J + \gamma$ ($n > n'$) and $n^3P_J \rightarrow n'^3S_1 + \gamma$ ($n \geq n'$) decays.

VI. RADIATIVE M1 TRANSITIONS

A. M1 decay rates

The radiative M1 transition rate is given by [14]

$$\Gamma(B \rightarrow A + \gamma) = \frac{\omega^3}{3\pi} (2J' + 1) |\mathcal{M}_{BA}|^2, \quad \text{where } \omega = \frac{M_B^2 - M_A^2}{2M_B}, \quad (37)$$

M_B and M_A are the initial and final meson masses, J' is the total angular momentum of the final meson. The matrix element of the magnetic moment \mathcal{M} is defined by

$$\mathcal{M}_{BA} = -\frac{i}{2} \left[\frac{\partial}{\partial \Delta} \times \langle A | \mathbf{J}(0) | B \rangle \right]_{\Delta=0}, \quad \Delta = \mathbf{P} - \mathbf{Q}, \quad (38)$$

where $\langle A | J_\mu(0) | B \rangle$ is the matrix element of the electromagnetic current between initial (B) and final (A) meson states with momenta \mathbf{Q} and \mathbf{P} , respectively.

After inserting the vertex functions $\Gamma^{(1)}$ and $\Gamma^{(2)}$ from Eqs. (33) and (34) in the decay matrix element (31) with the account of the wave function transformation (35), we carry out the expansion in inverse powers of the heavy meson masses $M_{B,A}$, which are large due to the presence of two heavy quarks $M_{B,A} \sim m_Q + m_{Q'}$. Then we calculate the matrix element of the magnetic moment operator (38) and get

(a) for the vector potential

$$\begin{aligned} \mathcal{M}_V = & \int \frac{d^3p}{(2\pi)^3} \bar{\Psi}_A(\mathbf{p}) \frac{e_1}{2\epsilon_1(p)} \left\{ \boldsymbol{\sigma}_1 + \frac{(1-\varepsilon)(1+2\kappa)[\mathbf{p} \times [\boldsymbol{\sigma}_1 \times \mathbf{p}]]}{2\epsilon_1(p)[\epsilon_1(p) + m_1]} \right. \\ & + \frac{(1-\varepsilon)(1+\kappa)[\mathbf{p} \times [\boldsymbol{\sigma}_2 \times \mathbf{p}]]}{\epsilon_1(p)[\epsilon_2(p) + m_2]} \\ & - \frac{\epsilon_2(p)}{M_B} \left(1 + (1-\varepsilon) \frac{M_B - \epsilon_1(p) - \epsilon_2(p)}{\epsilon_1(p)} \right) i \left[\mathbf{p} \times \frac{\partial}{\partial \mathbf{p}} \right] \\ & \left. + \frac{1}{2M_B} \left[\mathbf{p} \times \left[\mathbf{p} \times \left(\frac{\boldsymbol{\sigma}_1}{\epsilon_1(p) + m_1} - \frac{\boldsymbol{\sigma}_2}{\epsilon_2(p) + m_2} \right) \right] \right] \right\} \Psi_B(\mathbf{p}) + (1 \leftrightarrow 2), \quad (39) \end{aligned}$$

(b) for the scalar potential

$$\begin{aligned} \mathcal{M}_S = & \int \frac{d^3p}{(2\pi)^3} \bar{\Psi}_A(\mathbf{p}) \frac{e_1}{2\epsilon_1(p)} \left\{ \left(1 + \varepsilon \frac{\epsilon_1(p) + \epsilon_2(p) - M_B}{\epsilon_1(p)} \right) \right. \\ & \times \left(\boldsymbol{\sigma}_1 - \frac{\epsilon_2(p)}{M_B} i \left[\mathbf{p} \times \frac{\partial}{\partial \mathbf{p}} \right] \right) - \frac{\varepsilon [\mathbf{p} \times [\boldsymbol{\sigma}_1 \times \mathbf{p}]]}{2\epsilon_1(p)[\epsilon_1(p) + m_1]} \\ & \left. + \frac{1}{2M_B} \left[\mathbf{p} \times \left[\mathbf{p} \times \left(\frac{\boldsymbol{\sigma}_1}{\epsilon_1(p) + m_1} - \frac{\boldsymbol{\sigma}_2}{\epsilon_2(p) + m_2} \right) \right] \right] \right\} \Psi_B(\mathbf{p}) + (1 \leftrightarrow 2). \quad (40) \end{aligned}$$

Note that the last terms in Eqs. (39), (40) result from the wave function transformation (35) from the moving reference frame to the rest one. It is easy to see that in the limit $p/m \rightarrow 0$ the usual nonrelativistic expression for the magnetic moment follows.

Since we are interested in radiative transitions between S state (vector and pseudoscalar) mesons, it is possible to evaluate spin matrix elements using the relation $\langle \boldsymbol{\sigma}_1 \rangle = -\langle \boldsymbol{\sigma}_2 \rangle$.

Then, taking into account that both quarks are heavy (Q and Q'), we further expand Eqs. (39), (40) in inverse powers of the heavy quark mass m_Q up to the second order corrections to the leading contribution and get

(a) for the purely vector potential ($\varepsilon = 0$)

$$\mathcal{M}_V = \frac{e_Q}{2m_Q} \left\{ 1 - \frac{2\langle \mathbf{p}^2 \rangle}{3m_Q^2} + \frac{1 + \kappa \langle \mathbf{p}^2 \rangle}{3} \frac{1}{m_Q} \left(\frac{1}{m_Q} - \frac{1}{m_{Q'}} \right) - \frac{\langle \mathbf{p}^2 \rangle}{6M_B} \left(\frac{1}{m_Q} + \frac{1}{m_{Q'}} \right) \right\} - (Q \leftrightarrow Q'), \quad (41)$$

(b) for the purely scalar potential ($\varepsilon = 1$)

$$\mathcal{M}_S = \frac{e_Q}{2m_Q} \left\{ 2 - \frac{M_B - m_{Q'}}{m_Q} + \frac{\langle \mathbf{p}^2 \rangle}{2m_Q} \left(\frac{1}{m_{Q'}} - \frac{1}{3m_Q} \right) - \frac{\langle \mathbf{p}^2 \rangle}{6M_B} \left(\frac{1}{m_Q} + \frac{1}{m_{Q'}} \right) \right\} - (Q \leftrightarrow Q'). \quad (42)$$

Here $\langle \dots \rangle$ denotes the matrix element between radial meson wave functions. For these matrix element calculations we use the meson wave functions obtained calculating their mass spectra.

For the quarks of the same flavour ($m_Q = m_{Q'}$, $e_Q = -e_{\bar{Q}'}$) and $\kappa = -1$ these expressions reduce further [14]

(a) for the purely vector potential ($\varepsilon = 0$)

$$\mathcal{M}_V = 2 \frac{e_Q}{2m_Q} \left\{ 1 - \frac{2\langle \mathbf{p}^2 \rangle}{3m_Q^2} - \frac{\langle \mathbf{p}^2 \rangle}{3M_B m_Q} \right\}, \quad (43)$$

(b) for the purely scalar potential ($\varepsilon = 1$)

$$\mathcal{M}_S = 2 \frac{e_Q}{2m_Q} \left\{ 3 - \frac{M_B}{m_Q} + \frac{\langle \mathbf{p}^2 \rangle}{3m_Q} - \frac{\langle \mathbf{p}^2 \rangle}{3M_B m_Q} \right\}. \quad (44)$$

B. Results and discussion

The resulting $M1$ radiative decay rates of charmonium, bottomonium and B_c are presented in Tables V-VII. In these Tables we give predictions both for allowed ($n^3S_1 \rightarrow n'^1S_0 + \gamma$, $n' = n$) and hindered ($n > n'$) decays. For the calculation of allowed decay rates we use expanded expressions (41)–(44). For the hindered transitions, which are strongly suppressed in the nonrelativistic limit due to orthogonality of the initial and final state wave functions, relativistic effects are decisive. Thus for their calculations we use unexpanded expressions (39) and (40). In Tables V-VII we present the photon energy ω , the decay rates calculated discarding all relativistic corrections Γ^{NR} , as well as using relativistic expressions for purely vector Γ^V , for purely scalar Γ^S and for the mixture (9) of vector and scalar potentials Γ with $\varepsilon = -1$. Note that in all these calculations we use the relativistic wave functions found calculating the meson mass spectra in Sec. III.

The $M1$ radiative decay rates are very sensitive to relativistic effects. Even for allowed transitions relativistic and nonrelativistic results differ significantly. An important example is the decay $J/\Psi \rightarrow \eta_c \gamma$. It is well known that the nonrelativistic predictions for its rate are more than two times larger than the experimental data. As we see from Table V, the inclusion of the relativistic corrections for purely scalar or purely vector potentials do not bring theoretical results in agreement with experiment. For the purely scalar potential the decay

TABLE V: Radiative M1 decay rates of charmonium. For decays involving η'_c we give in parenthesis the results obtained using the recent value [23] of its mass. The values Γ^{exp} are taken from Ref. [22].

Decay	ω MeV	Γ^{NR} keV	Γ^V keV	Γ^S keV	Γ keV	Γ^{exp} keV
$J/\Psi \rightarrow \eta_c \gamma$	115	2.73	1.95	3.13	1.05	1.13 ± 0.35
$\Psi' \rightarrow \eta'_c \gamma$	91(32)	1.26(0.055)	0.85(0.037)	0.71(0.031)	0.99(0.043)	$0.6 - 3.9^a$
$\Psi' \rightarrow \eta_c \gamma$	639	0.23	0.61	0.35	0.95	0.84 ± 0.19
$\eta'_c \rightarrow J/\Psi \gamma$	463(514)	0.26(0.36)	0.70(0.95)	0.37(0.51)	1.12(1.53)	

^aThis value from Ref. [24] needs confirmation and is included only in the PDG Listings.

TABLE VI: Radiative M1 decay rates of bottomonium.

Decay	ω MeV	Γ^{NR} eV	Γ^V eV	Γ^S eV	Γ eV	\mathcal{B} (10^{-4})
$\Upsilon \rightarrow \eta_b \gamma$	60	9.7	8.7	12.2	5.8	1.1
$\Upsilon' \rightarrow \eta'_b \gamma$	33	1.6	1.45	1.50	1.40	0.32
$\Upsilon'' \rightarrow \eta''_b \gamma$	27	0.9	0.8	0.8	0.8	0.30
$\Upsilon' \rightarrow \eta_b \gamma$	604	1.3	3.4	1.3	6.4	1.5
$\eta'_b \rightarrow \Upsilon \gamma$	516	2.4	6.3	2.5	11.8	
$\Upsilon'' \rightarrow \eta_b \gamma$	911	2.5	6.2	3.1	10.5	4.0
$\eta''_b \rightarrow \Upsilon \gamma$	831	5.8	14.3	7.1	24.0	
$\Upsilon'' \rightarrow \eta'_b \gamma$	359	0.2	0.6	0.1	1.5	0.57
$\eta''_b \rightarrow \Upsilon' \gamma$	301	0.4	1.1	0.2	2.8	

rate even increases by 15%. On the other hand for the purely vector potential relativistic effects decrease the decay rate by 25%, but such decrease is not enough: the theoretical result still deviates from experimental data by more than 2σ .³ Only for the mixture of vector and scalar potentials (9) we get the necessary decrease of the decay rate which brings theory in agreement with experimental data for the $J/\Psi \rightarrow \eta_c \gamma$ decay rate. For the hindered

TABLE VII: Radiative M1 decay rates of the B_c meson.

Transition	ω MeV	Γ^{NR} eV	Γ^V eV	Γ^S eV	Γ eV	Γ [33] eV	Γ [34] eV	Γ [35] eV
$1^3S_1 \rightarrow 1^1S_0 \gamma$	62	73	48	66	33	135	60	59
$2^3S_1 \rightarrow 2^1S_0 \gamma$	46	30	24	32	17	29	10	12
$2^3S_1 \rightarrow 1^1S_0 \gamma$	584	141	412	398	428	123	98	122
$2^1S_0 \rightarrow 2^3S_1 \gamma$	484	160	471	454	488	93	96	139

³ This is compatible with the estimate that relativistic effects can give contributions of order of 20–30% in charmonium.

decay $\Psi' \rightarrow \eta_c \gamma$ the decay rate calculated for the mixture of vector and scalar potentials is also in good agreement with experiment while the rates for pure potentials (especially the scalar one) are lower than the experimental value. In Table V we give predictions for decays involving the first radial excitation of the pseudoscalar state $\eta'_c(2^1S_0)$ as well. Since there are two contradicting experimental measurements of its mass we calculated the rates using both values. The results obtained using recent Belle value [23] are given in parenthesis.

In Table VI predictions for M1 decay rates and branching fractions of bottomonium are given. Since the hyperfine splitting in bottomonium is predicted to be small (around 60 MeV, see Table II) the photon energies and hence decay rates of allowed M1 transitions are very small. This is one of the main reasons why no spin-singlet S -wave levels $\eta_b(n^1S_0)$ have been observed yet. Our results show that relativistic effects for the favored mixture of vector and scalar potentials further decrease the allowed M1 decay rates.

Recently it was argued by Godfrey and Rosner [4] that hindered transitions could be more favorable for discovering the η_b . Their analysis of different quark model predictions showed that most nonrelativistic models favor the $\eta_b(1S)$ production from $\Upsilon(2S)$ decays, while the account of relativistic corrections makes prospects for discovering $\eta_b(1S)$ in $\Upsilon(3S)$ radiative decays comparable to those in $\Upsilon(2S)$ decays. Our present relativistic consideration of these decays supports this observation. Indeed we see from Table VI that relativistic effects significantly increase rates of hindered transitions. The hindered decay $\Upsilon''(3S) \rightarrow \eta_b(1S)\gamma$ has the largest branching fraction 4.0×10^{-4} , which is almost 2.7 times larger than the $\Upsilon'(2S) \rightarrow \eta_b(1S)\gamma$ decay branching fraction. Very recently CLEO Collaboration [42] searched for $\eta_b(1S)$ in such hindered M1 transition from $\Upsilon''(3S)$. No evidence of $\Upsilon''(3S) \rightarrow \eta_b(1S)\gamma$ transitions was found and rather strict upper limits on the branching fraction were set: $\mathcal{B}(\Upsilon''(3S) \rightarrow \eta_b(1S)\gamma) < 6 \times 10^{-4}$, which rule out many previous phenomenological predictions reviewed in Ref. [4]. Our model result for the branching fraction of this decay is below but rather close to this experimental upper limit.

In Table VII we give predictions for decay rates of M1 radiative transitions of the B_c meson in our model in comparison with previous nonrelativistic quark model analysis [33, 34, 35]. We see that relativistic effects play an important role in B_c meson M1 radiative decays. They reduce the rates of allowed decays and increase the rates of hindered transitions. The largest rates are predicted for the latter decays which are increased by relativistic effects almost by the factor of 3 and thus they are an order of magnitude larger than the rates of allowed M1 transitions.

VII. RADIATIVE E1 TRANSITIONS

A. E1 decay rates

The radiative E1 transition rate is given by [43]

$$\Gamma(B \rightarrow A + \gamma) = \frac{\omega^3}{3\pi} |\mathbf{D}_{BA}|^2, \quad \text{where} \quad \omega = \frac{M_B^2 - M_A^2}{2M_B}, \quad (45)$$

M_B and M_A are the initial and final meson masses. The matrix element of the electric dipole moment \mathbf{D}_{BA} is defined by

$$\mathbf{D}_{BA} = -i \frac{\partial}{\partial \Delta} \langle A | J_0(0) | B \rangle \Big|_{\Delta=0}, \quad \Delta = \mathbf{P} - \mathbf{Q}, \quad (46)$$

where $\langle A | J_\mu(0) | B \rangle$ is the matrix element of the electromagnetic current between initial (B) and final (A) meson states with momenta \mathbf{Q} and \mathbf{P} , respectively.

We substitute expressions (31)–(34) in the definition of the electric dipole moment (46) and take into account the relativistic transformation of the wave function (35). Then, discarding some terms of order v^4/c^4 and higher, we get the following expressions for the electric dipole moment \mathbf{D}_{BA} [43] (indices 1,2 are changed to Q, Q')

(a) for the purely vector potential

$$\mathbf{D}_V = \int \frac{d^3p}{(2\pi)^3} \bar{\Psi}_A(\mathbf{p}) e_Q \left\{ i \frac{\epsilon_{Q'}(p)}{M_B} \frac{\partial}{\partial \mathbf{p}} - \frac{[\boldsymbol{\sigma}_Q \times \mathbf{p}]}{2\epsilon_Q(p)[\epsilon_Q(p) + m_Q]} \left(1 - \frac{\epsilon_Q(p)}{M_B} + \frac{2[M_B - \epsilon_Q(p) - \epsilon_{Q'}(p)]}{m_Q} \right) - \frac{[\boldsymbol{\sigma}_{Q'} \times \mathbf{p}]}{2M_B[\epsilon_{Q'}(p) + m_{Q'}]} \right\} \Psi_B(\mathbf{p}) - (Q \leftrightarrow Q'), \quad (47)$$

(b) for the purely scalar potential

$$\mathbf{D}_S = \int \frac{d^3p}{(2\pi)^3} \bar{\Psi}_A(\mathbf{p}) e_Q \left\{ i \frac{\epsilon_{Q'}(p)}{M_B} \frac{\partial}{\partial \mathbf{p}} - \frac{[\boldsymbol{\sigma}_Q \times \mathbf{p}]}{2\epsilon_Q(p)[\epsilon_Q(p) + m_Q]} \left(1 - \frac{\epsilon_Q(p)}{M_B} - \frac{2[M_B - \epsilon_Q(p) - \epsilon_{Q'}(p)]}{m_Q} \right) - \frac{[\boldsymbol{\sigma}_{Q'} \times \mathbf{p}]}{2M_B[\epsilon_{Q'}(p) + m_{Q'}]} \right\} \Psi_B(\mathbf{p}) - (Q \leftrightarrow Q'). \quad (48)$$

The operator $i\partial/\partial\mathbf{p}$ in Eqs. (47), (48) corresponds in the coordinate space to the operator \mathbf{r} . All other terms in these equations are relativistic corrections. Thus in the nonrelativistic limit the standard expression for the electric dipole moment is recovered.

It is easy to see that there are three different structures with respect to the orbital variables in Eqs. (47), (48): \mathbf{r} , $[(\boldsymbol{\sigma}_Q + \boldsymbol{\sigma}_{Q'}) \times \mathbf{p}]$ and $[(\boldsymbol{\sigma}_Q - \boldsymbol{\sigma}_{Q'}) \times \mathbf{p}]$. Thus the matrix element of the electric dipole moment for the electromagnetic transition $nJMLS \rightarrow n'J'M'L'S' + \gamma$ can be presented in the form

$$\mathbf{D}_{V,S} = \langle n'J'M'L'S' | \mathcal{A}(p^2) \mathbf{r} - \mathcal{B}^{V,S}(p^2) [\mathbf{S} \times \mathbf{p}] - \mathcal{C}^{V,S}(p^2) [(\mathbf{S}_Q - \mathbf{S}_{Q'}) \times \mathbf{p}] | nJMLS \rangle, \quad (49)$$

where functions $\mathcal{A}(p^2)$, $\mathcal{B}^{V,S}(p^2)$ and $\mathcal{C}^{V,S}(p^2)$ up to order $\mathbf{p}^2/m_{Q(Q')}^2$ are given by

$$\begin{aligned} \mathcal{A}(p^2) &= \frac{e_Q m_{Q'} - e_{Q'} m_Q}{M_B} + \frac{e_Q m_Q - e_{Q'} m_{Q'}}{M_B} \frac{\mathbf{p}^2}{2m_Q m_{Q'}}, \quad (50) \\ \mathcal{B}^V(p^2) &= \frac{e_Q}{4m_Q^2} \left(1 + \frac{2(M - m_Q - m_{Q'})}{m_Q} - \frac{7\mathbf{p}^2}{4m_Q^2} - \frac{\mathbf{p}^2}{m_{Q'}^2} \right) \\ &\quad - \frac{e_{Q'}}{4m_{Q'}^2} \left(1 + \frac{2(M - m_Q - m_{Q'})}{m_{Q'}} - \frac{7\mathbf{p}^2}{4m_{Q'}^2} - \frac{\mathbf{p}^2}{m_Q^2} \right) \\ &\quad - \frac{e_Q + e_{Q'}}{4M_B} \left[\frac{1}{m_Q} - \frac{1}{m_{Q'}} - \frac{\mathbf{p}^2}{4} \left(\frac{1}{m_Q^3} - \frac{1}{m_{Q'}^3} \right) \right], \quad (51) \\ \mathcal{C}^V(p^2) &= \frac{e_Q}{4m_Q^2} \left(1 + \frac{2(M - m_Q - m_{Q'})}{m_Q} - \frac{7\mathbf{p}^2}{4m_Q^2} - \frac{\mathbf{p}^2}{m_{Q'}^2} \right) \\ &\quad + \frac{e_{Q'}}{4m_{Q'}^2} \left(1 + \frac{2(M - m_Q - m_{Q'})}{m_{Q'}} - \frac{7\mathbf{p}^2}{4m_{Q'}^2} - \frac{\mathbf{p}^2}{m_Q^2} \right) \end{aligned}$$

$$-\frac{e_Q + e_{Q'}}{4M_B} \left[\frac{1}{m_Q} + \frac{1}{m_{Q'}} - \frac{\mathbf{p}^2}{4} \left(\frac{1}{m_Q^3} + \frac{1}{m_{Q'}^3} \right) \right], \quad (52)$$

$$\begin{aligned} \mathcal{B}^S(p^2) &= \frac{e_Q}{4m_Q^2} \left(1 - \frac{2(M - m_Q - m_{Q'})}{m_Q} + \frac{\mathbf{p}^2}{4m_Q^2} + \frac{\mathbf{p}^2}{m_Q m_{Q'}} \right) \\ &\quad - \frac{e_{Q'}}{4m_{Q'}^2} \left(1 - \frac{2(M - m_Q - m_{Q'})}{m_{Q'}} + \frac{\mathbf{p}^2}{4m_{Q'}^2} + \frac{\mathbf{p}^2}{m_Q m_{Q'}} \right) \\ &\quad - \frac{e_Q + e_{Q'}}{4M_B} \left[\frac{1}{m_Q} - \frac{1}{m_{Q'}} - \frac{\mathbf{p}^2}{4} \left(\frac{1}{m_Q^3} - \frac{1}{m_{Q'}^3} \right) \right], \end{aligned} \quad (53)$$

$$\begin{aligned} \mathcal{C}^S(p^2) &= \frac{e_Q}{4m_Q^2} \left(1 - \frac{2(M - m_Q - m_{Q'})}{m_Q} + \frac{\mathbf{p}^2}{4m_Q^2} + \frac{\mathbf{p}^2}{m_Q m_{Q'}} \right) \\ &\quad + \frac{e_{Q'}}{4m_{Q'}^2} \left(1 - \frac{2(M - m_Q - m_{Q'})}{m_{Q'}} + \frac{\mathbf{p}^2}{4m_{Q'}^2} + \frac{\mathbf{p}^2}{m_Q m_{Q'}} \right) \\ &\quad - \frac{e_Q + e_{Q'}}{4M_B} \left[\frac{1}{m_Q} + \frac{1}{m_{Q'}} - \frac{\mathbf{p}^2}{4} \left(\frac{1}{m_Q^3} + \frac{1}{m_{Q'}^3} \right) \right]. \end{aligned} \quad (54)$$

The last structure in Eq. (49) proportional to $[(\mathbf{S}_Q - \mathbf{S}_{Q'}) \times \mathbf{p}]$ leads to the spin-flip transitions. It vanishes for the $c\bar{c}$ and $b\bar{b}$ mesons, consisting of the quark and antiquark of the same flavour ($m_Q = m_{Q'}$, $e_Q = -e_{Q'}$) since in that case $\mathcal{C}^{V,S}(p^2) = 0$. The functions $\mathcal{A}(p^2)$, $\mathcal{B}^{V,S}(p^2)$ then simplify and coincide with the ones found previously [43]

$$\begin{aligned} \mathcal{A}(p^2) &= e_Q \left(\frac{2m_Q}{M_B} + \frac{\mathbf{p}^2}{M_B m_Q} \right), \\ \mathcal{B}^V(p^2) &= \frac{e_Q}{2m_Q^2} \left(1 + \frac{2(M_B - 2m_Q)}{m_Q} - \frac{11\mathbf{p}^2}{4m_Q^2} \right), \\ \mathcal{B}^S(p^2) &= \frac{e_Q}{2m_Q^2} \left(1 - \frac{2(M_B - 2m_Q)}{m_Q} + \frac{5\mathbf{p}^2}{4m_Q^2} \right). \end{aligned}$$

In the case of the B_c meson $\mathcal{C}^{V,S}(p^2) \neq 0$ and thus relativistic corrections lead to spin-flip transitions ($S' = S \pm 1$) but only for decays involving mixed states $nP1$, $nP1'$ (24) or $nD2$, $nD2'$ (25). For all other transitions the spin-flip correction vanishes due to momenta relations (see Eq. (57) below).

Using the Wigner-Eckart theorem and relations for matrix elements of the tensor operator between coupled functions, one can rewrite Eq. (49) in the form

$$\begin{aligned} D_i &= (-1)^{J'+J+L+S-M'} \begin{pmatrix} J' & 1 & J \\ -M' & i & M \end{pmatrix} \sqrt{(2J+1)(2J'+1)} \\ &\quad \times \left[\left\{ \begin{matrix} L' & J' & S \\ J & L & 1 \end{matrix} \right\} \delta_{SS'} \left(\langle n'L' || \mathcal{A}(p^2)r || nL \rangle - \eta(J', L', J, L, S) \langle n'L' || \mathcal{B}(p^2)p || nL \rangle \right) \right. \\ &\quad \left. - \chi(J', L', J, L) \delta_{SS' \pm 1} \langle n'L' || \mathcal{C}(p^2)p || nL \rangle \right], \end{aligned} \quad (55)$$

where

$$\eta(J', L', J, L, S) = (-1)^{L+J+1} \sqrt{6} [S(S+1)(2S+1)]^{1/2} \left(\begin{Bmatrix} L' & J' & S \\ J & L & 1 \end{Bmatrix} \right)^{-1} \begin{Bmatrix} J & S & L \\ J' & S & L' \\ 1 & 1 & 1 \end{Bmatrix}, \quad (56)$$

$$\chi(J', L', J, L) = (-1)^{L+L'} \sqrt{\frac{2}{2J'+1}} \begin{Bmatrix} J & L & 1 \\ 1 & 1 & L' \end{Bmatrix}. \quad (57)$$

Here

$$\begin{pmatrix} J' & 1 & J \\ -M' & q & M \end{pmatrix}, \quad \begin{Bmatrix} L' & J' & S \\ J & L & 1 \end{Bmatrix}, \quad \text{and} \quad \begin{Bmatrix} J & S & L \\ J' & S & L' \\ 1 & 1 & 1 \end{Bmatrix}$$

are $3j$ -, $6j$ - and $9j$ -symbols, $\langle n'L' || \dots || nL \rangle$ are reduced matrix elements.

The total E1 decay rate of the $nJLS$ state is obtained by summing the decay rates (45) over all possible values of M' for a fixed value of M . The resulting expression is

$$\begin{aligned} \Gamma^{V,S}(nJLS \rightarrow n'J'L'S' + \gamma) &= \frac{4}{3} \alpha \omega^3 \left\{ \delta_{SS'} C^{1/2}(J', L', J, L, S) \left[(L' - L) \langle R_{n'L'} | \mathcal{A}(p^2)r | R_{nL} \rangle \right. \right. \\ &\quad \left. \left. - \frac{\eta(J', L', J, L, S)}{\sqrt{\max(L', L)}} \langle n'L' || \mathcal{B}^{V,S}(p^2)p || nL \rangle \right] \right. \\ &\quad \left. - \delta_{SS' \pm 1} \chi(J', L', J, L) \langle n'L' || \mathcal{C}^{V,S}(p^2)p || nL \rangle \right\}^2, \quad (58) \end{aligned}$$

where

$$C(J', L', J, L, S) = \max(L', L)(2J' + 1) \begin{Bmatrix} L' & J' & S \\ J & L & 1 \end{Bmatrix}^2.$$

The reduced matrix elements can be expressed through the usual matrix elements over radial wave functions $R_{nL}(r)$:

(a) for the transitions between P and S states

$$\langle n'0 || p || n1 \rangle = -\langle R'_{n'S} | R_{nP} \rangle,$$

$$\langle n'0 || \mathbf{p}^2 p || n1 \rangle = \langle R'''_{n'S} | R_{nP} \rangle + 2 \left\langle R''_{n'S} \left| \frac{1}{r} \right| R_{nP} \right\rangle - 2 \left\langle R'_{n'S} \left| \frac{1}{r^2} \right| R_{nP} \right\rangle; \quad (59)$$

(b) for the transitions between D and P states

$$\langle n'1 || p || n2 \rangle = -\sqrt{2} \left(\left\langle R'_{n'P} \left| \frac{1}{r} \right| R_{nD} \right\rangle - \langle R'_{n'P} | R_{nD} \rangle \right),$$

$$\begin{aligned} \langle n'1 || \mathbf{p}^2 p || n2 \rangle &= -\sqrt{2} \left(\langle R'''_{n'P} | R_{nD} \rangle + \left\langle R''_{n'P} \left| \frac{1}{r} \right| R_{nD} \right\rangle \right. \\ &\quad \left. - 6 \left\langle R'_{n'P} \left| \frac{1}{r^2} \right| R_{nD} \right\rangle + 6 \left\langle R_{n'P} \left| \frac{1}{r^3} \right| R_{nD} \right\rangle \right), \quad (60) \end{aligned}$$

where the prime means differentiation of R with respect to r .

TABLE VIII: Radiative E1 transition rates of charmonium. For decays involving η'_c we give in parenthesis the results obtained using the recent value [23] of its mass.

Decay	ω MeV	Γ^{NR} keV	Γ^V keV	Γ^S keV	Γ keV	Γ^{exp} [22] keV
$2^3S_1 \rightarrow 1^3P_0\gamma$	259	51.7	34.6	44.0	26.3	26.1 ± 3.2
$2^3S_1 \rightarrow 1^3P_1\gamma$	171	44.9	30.1	38.3	22.9	25.2 ± 3.0
$2^3S_1 \rightarrow 1^3P_2\gamma$	128	30.9	22.9	28.1	18.2	20.4 ± 2.5
$2^1S_0 \rightarrow 1^1P_1\gamma$	68(128)	8.6(57)	6.2(41)	6.2(41)	6.2(41)	
$1^3P_0 \rightarrow 1^3S_1\gamma$	305	161	151	184	121	165 ± 36
$1^3P_1 \rightarrow 1^3S_1\gamma$	389	333	285	305	265	291 ± 51
$1^3P_2 \rightarrow 1^3S_1\gamma$	430	448	309	292	327	389 ± 52
$1^1P_1 \rightarrow 1^1S_0\gamma$	504	723	560	560	560	
$1^3D_1 \rightarrow 1^3P_0\gamma$	361	423	344	334	355	
$1^3D_1 \rightarrow 1^3P_1\gamma$	277	142	127	120	135	
$1^3D_1 \rightarrow 1^3P_2\gamma$	234	5.8	6.2	5.6	6.9	
$1^3D_2 \rightarrow 1^3P_1\gamma$	291	297	215	215	215	
$1^3D_2 \rightarrow 1^3P_2\gamma$	248	62	55	51	59	
$1^3D_3 \rightarrow 1^3P_2\gamma$	250	252	163	170	156	
$1^1D_2 \rightarrow 1^1P_1\gamma$	275	335	245	245	245	

B. Results and discussion

The results of numerical calculations of charmonium E1 radiative decay rates using Eqs. (56)–(60) are presented in Table VIII. For calculations of photon energies ω we used the experimentally measured masses of charmonium S and P states.⁴ For masses of D states we used our model predictions from Table I. We give predictions for decay rates calculated in the nonrelativistic limit Γ^{NR} , for relativistic decay rates with pure vector Γ^V and scalar Γ^S potentials as well as for the mixture (9) of vector and scalar potentials Γ with $\varepsilon = -1$. As in the case of M1 decay rates calculations, we use the relativistic wave functions in our numerical analysis.

The results presented in Table VIII show that relativistic effects play an important role in E1 decays of charmonium. The most sensitive to the relativistic corrections are decays $\Psi'(2S) \rightarrow \chi_{cJ}(1P) + \gamma$. Their account leads to the considerable reduction of the decay rates. The rates for the vector potential are reduced more significantly than for the scalar one. As a result, there arises an approximately twofold reduction of decay rates for the mixture of vector and scalar potentials with the value of mixing parameter $\varepsilon = -1$, bringing theoretical predictions in good agreement with experimental data. The large influence of relativistic corrections originates from the fact that the zero of the $2S$ wave function is close to the maximum of the $1P$ wave function. This results in a reduction of the leading order decay matrix element $\langle 1P|r|2S \rangle$. Therefore relatively small relativistic corrections produce

⁴ For decays involving $\eta'_c(2S)$, as in the case of M1 transitions, we use both experimental values of its mass, giving a prediction for the recent Belle value [23] in parenthesis.

such a large effect. This observation is confirmed by the calculations of the $\chi_{cJ}(1P) \rightarrow J/\Psi + \gamma$ decay rates. Here both initial and final states do not have zeros and relativistic contributions have usual values and lead to an approximately 25% reduction of the decay rate. All theoretical predictions are in nice agreement with data. In Table VIII we also give predictions for E1 decay rates of charmonium $1D$ states. At present only the 1^3D_1 state is experimentally observed. This state is considerably broader, since it lies above the $D\bar{D}$ threshold. The observed state $\Psi(3770)$ can also have a significant 2^3S_1 state admixture [44]. If we consider it to be a pure D state, then using its measured total decay rate, we get the following predictions for the E1 radiative decay branching fractions:

$$\mathcal{B}(1^3D_1 \rightarrow 1^3P_0\gamma) \approx 1.5\%; \quad \mathcal{B}(1^3D_1 \rightarrow 1^3P_1\gamma) \approx 0.6\%; \quad \mathcal{B}(1^3D_1 \rightarrow 1^3P_2\gamma) \approx 0.03\%.$$

On the other hand, the tensor 1^3D_2 and 1^1D_2 charmonium states are under the threshold of open charm production, since their masses are slightly below the $D\bar{D}^*$ threshold, and the decay of these states to $D\bar{D}$ is forbidden by parity and angular momentum conservation. Thus E1 radiative transitions are the main decay channels of these states.

The calculated decay rates of E1 radiative transitions in bottomonium are presented in Tables IX and X. The influence of relativistic effects in bottomonium is considerably less than in charmonium. The contribution of relativistic corrections does not exceed 10% almost for all decays. The only exceptions are decays $\Upsilon''(3S) \rightarrow \chi_{bJ}(1P) + \gamma$, where the leading contribution is substantially reduced due to the significantly different number of zeros in initial $3S$ and final $1P$ wave functions. For all $S \rightarrow P + \gamma$ transitions we find good agreement of our model predictions with experimental data.

The comparison of the theoretical predictions for the radiative decays of P states of bottomonium $\chi_b(nP)$ with the experimental data is complicated by the fact that the total decay rates of these states are not measured yet. Experiment gives only branching fractions $\mathcal{B} \equiv \Gamma[\chi_b(nP) \rightarrow \Upsilon(n'S) + \gamma]/\Gamma^{\text{total}}$ ($n \geq n'$) for these decays. Thus for this comparison it is necessary to get theoretical predictions for the total decay rates of $\chi_b(nP)$. The main decay channels of the bottomonium P states are inclusive strong decays to gluon and quark states and radiative decays. The strong decays were extensively studied in the literature [45, 46] including leading-order QCD corrections. The two-gluon annihilation rates of 3P_0 states with the account of relativistic corrections are given in our model [47] by

$$\begin{aligned} \Gamma(^3P_0 \rightarrow gg) = & \frac{8\alpha_s^2}{3M^2} \left| \int \frac{d^3p}{(2\pi)^3} \frac{m_Q^2}{Mp} \left[\frac{p}{\epsilon_Q(p)} \ln \frac{\epsilon_Q(p) + p}{\epsilon_Q(p) - p} \right. \right. \\ & \left. \left. + \left(1 - \frac{M}{2\epsilon_Q(p)} \right) \left(2 - \frac{\epsilon_Q(p)}{p} \ln \frac{\epsilon_Q(p) + p}{\epsilon_Q(p) - p} \right) \right] \phi_P(p) \right|^2. \end{aligned} \quad (61)$$

To include leading-order QCD corrections [46] this expression should be multiplied by $(1 + 10.0\alpha_s/\pi)$ for χ_{b0} and $(1 + 10.2\alpha_s/\pi)$ for χ'_{b0} . The corresponding expression for two-gluon annihilation rates of 3P_2 states reads as [47]

$$\begin{aligned} \Gamma(^3P_2 \rightarrow gg) = & \frac{8\alpha_s^2}{5M^2} \left\{ \left| \int \frac{d^3p}{(2\pi)^3} \frac{m_Q \epsilon_Q(p)}{Mp} \left[\left(2 + \frac{p}{\epsilon_Q(p)} \ln \frac{\epsilon_Q(p) + p}{\epsilon_Q(p) - p} - \frac{\epsilon_Q(p)}{p} \ln \frac{\epsilon_Q(p) + p}{\epsilon_Q(p) - p} \right) \right. \right. \right. \\ & \left. \left. \times \left(1 + \frac{m_Q}{2\epsilon_Q(p)[\epsilon_Q(p) + m_Q]} \right) - \frac{2p^2}{3\epsilon_Q(p)[\epsilon_Q(p) + m_Q]} \right] \phi_P(p) \right|^2 \end{aligned}$$

TABLE IX: Radiative E1 transition rates of bottomonium.

Decay	ω MeV	Γ^{NR} keV	Γ^V keV	Γ^S keV	Γ keV	Γ^{exp} [22] keV
$2^3S_1 \rightarrow 1^3P_0\gamma$	162	1.65	1.64	1.66	1.62	1.67 ± 0.37
$2^3S_1 \rightarrow 1^3P_1\gamma$	130	2.57	2.48	2.51	2.45	2.9 ± 0.6
$2^3S_1 \rightarrow 1^3P_2\gamma$	109	2.53	2.49	2.52	2.46	3.08 ± 0.6
$2^1S_0 \rightarrow 1^1P_1\gamma$	98	3.25	3.09	3.09	3.09	
$1^3P_0 \rightarrow 1^3S_1\gamma$	391	29.5	30.6	31.3	29.9	
$1^3P_1 \rightarrow 1^3S_1\gamma$	422	37.1	37.0	37.4	36.6	
$1^3P_2 \rightarrow 1^3S_1\gamma$	442	42.7	39.8	39.3	40.2	
$1^1P_1 \rightarrow 1^1S_0\gamma$	480	54.4	52.6	52.6	52.6	
$3^3S_1 \rightarrow 2^3P_0\gamma$	123	1.65	1.51	1.52	1.49	1.42 ± 0.25
$3^3S_1 \rightarrow 2^3P_1\gamma$	100	2.65	2.43	2.45	2.41	2.97 ± 0.43
$3^3S_1 \rightarrow 2^3P_2\gamma$	86	2.89	2.69	2.71	2.67	3.0 ± 0.45
$3^1S_0 \rightarrow 2^1P_1\gamma$	73	3.07	2.78	2.78	2.78	
$3^3S_1 \rightarrow 1^3P_0\gamma$	484	0.124	0.040	0.054	0.027	
$3^3S_1 \rightarrow 1^3P_1\gamma$	453	0.307	0.097	0.134	0.067	0.041 ± 0.029^a
$3^3S_1 \rightarrow 1^3P_2\gamma$	433	0.445	0.141	0.195	0.097	0.064 ± 0.045^a
$3^1S_0 \rightarrow 1^1P_1\gamma$	427	0.770	0.348	0.348	0.348	
$2^3P_0 \rightarrow 2^3S_1\gamma$	207	11.7	11.1	11.2	11.0	
$2^3P_1 \rightarrow 2^3S_1\gamma$	230	15.9	14.8	14.8	14.7	
$2^3P_2 \rightarrow 2^3S_1\gamma$	243	18.8	16.7	16.6	16.7	
$2^1P_1 \rightarrow 2^1S_0\gamma$	262	23.6	21.4	21.4	21.4	
$2^3P_0 \rightarrow 1^3S_1\gamma$	743	7.36	7.58	8.41	6.79	
$2^3P_1 \rightarrow 1^3S_1\gamma$	764	8.01	7.90	8.33	7.49	
$2^3P_2 \rightarrow 1^3S_1\gamma$	776	8.41	7.61	7.20	8.02	
$2^1P_1 \rightarrow 1^1S_0\gamma$	820	9.9	9.36	9.36	9.36	

^aNeeds confirmation.

$$\begin{aligned}
& + \frac{1}{6} \left| \int \frac{d^3p}{(2\pi)^3} \frac{m_Q^2}{Mp} \left[\frac{p}{\epsilon_Q(p)} \ln \frac{\epsilon_Q(p) + p}{\epsilon_Q(p) - p} + 3 \left(2 - \frac{\epsilon_Q(p)}{p} \ln \frac{\epsilon_Q(p) + p}{\epsilon_Q(p) - p} \right) \right. \right. \\
& - \frac{\epsilon_Q(p)}{m_Q} \left(2 - \frac{M}{m_Q} \right) \left(2 - \frac{\epsilon_Q(p)}{p} \ln \frac{\epsilon_Q(p) + p}{\epsilon_Q(p) - p} \right) + \frac{p^2}{m_Q[\epsilon_Q(p) + m_Q]} \left(2 - \frac{M}{m_Q} \right) \\
& \left. \left. \times \left(\frac{1}{2} \left(\frac{\epsilon_Q(p)}{p} \ln \frac{\epsilon_Q(p) + p}{\epsilon_Q(p) - p} - 2 \right) \left(1 - \frac{3\epsilon_Q^2(p)}{p^2} \right) + 1 \right) \right] \phi_P(p) \right|^2 \Bigg\}, \quad (62)
\end{aligned}$$

with leading-order QCD corrections [46] accounted by the factors $(1 - 0.1\alpha_s/\pi)$ for χ_{b2} and $(1 + 1.0\alpha_s/\pi)$ for χ'_{b2} . Here $\phi_P(p)$ is the P state radial wave function in momentum space. In the nonrelativistic limit $p/m_Q \rightarrow 0$ and $M \rightarrow 2m_Q$, Eqs. (61) and (62) reduce to the

TABLE X: Radiative E1 transition rates of bottomonium involving D states.

Decay	ω MeV	Γ^{NR} keV	Γ^V keV	Γ^S keV	Γ keV
$1^3D_1 \rightarrow 1^3P_0\gamma$	280	24.2	23.4	23.4	23.4
$1^3D_1 \rightarrow 1^3P_1\gamma$	256	12.9	12.7	12.7	12.7
$1^3D_1 \rightarrow 1^3P_2\gamma$	235	0.67	0.69	0.69	0.69
$1^3D_2 \rightarrow 1^3P_1\gamma$	262	24.8	23.3	23.3	23.3
$1^3D_2 \rightarrow 1^3P_2\gamma$	241	6.45	6.35	6.35	6.35
$1^3D_3 \rightarrow 1^3P_2\gamma$	244	26.7	24.6	24.6	24.6
$1^1D_2 \rightarrow 1^1P_1\gamma$	254	30.2	28.4	28.4	28.4
$2^3P_0 \rightarrow 1^3D_1\gamma$	81	1.17	1.16	1.16	1.17
$2^3P_1 \rightarrow 1^3D_1\gamma$	104	0.62	0.61	0.60	0.615
$2^3P_1 \rightarrow 1^3D_2\gamma$	98	1.56	1.56	1.56	1.56
$2^3P_2 \rightarrow 1^3D_1\gamma$	117	0.036	0.034	0.034	0.035
$2^3P_2 \rightarrow 1^3D_2\gamma$	111	0.454	0.446	0.443	0.449
$2^3P_2 \rightarrow 1^3D_3\gamma$	108	2.34	2.36	2.37	2.35
$2^1P_1 \rightarrow 1^1D_2\gamma$	102	2.62	2.43	2.43	2.43

known expressions [46]:

$$\Gamma(^3P_0 \rightarrow gg) = \frac{6\alpha_s^2 |R'_{nP}(0)|^2}{m_Q^4}, \quad (63)$$

$$\Gamma(^3P_2 \rightarrow gg) = \frac{8\alpha_s^2 |R'_{nP}(0)|^2}{5m_Q^4}. \quad (64)$$

The calculation of radiative and relativistic corrections to the annihilation decay rates of 3P_1 and 1P_1 states is a very complicated problem which has not been solved yet. Thus to estimate their hadronic decay rates we use the tree-level nonrelativistic expressions [46]

$$\Gamma(^3P_1 \rightarrow q\bar{q} + g) = \frac{8\alpha_s^3 n_f}{9\pi m_Q^4} |R'_{nP}(0)|^2 \ln(m_Q \langle r \rangle), \quad (65)$$

$$\Gamma(^1P_1 \rightarrow ggg) = \frac{20\alpha_s^3}{9\pi m_Q^4} |R'_{nP}(0)|^2 \ln(m_Q \langle r \rangle), \quad (66)$$

$$\Gamma(^1P_1 \rightarrow gg + \gamma) = \frac{36}{5} e_q^2 \frac{\alpha}{\alpha_s} \Gamma(^1P_1 \rightarrow ggg). \quad (67)$$

From the relativistic consideration of the decays of $^3P_{0,2}$ states, which shows that relativistic effects give $\sim 10\%$ contributions to the $b\bar{b}$ decay rates, we can expect that these formulae give a reasonable estimate of the corresponding decay rates. For numerical calculations of hadronic decay rates of χ_b states we use $\alpha_s = 0.18$ obtained from the experimental ratio $\Gamma(\Upsilon \rightarrow gg\gamma)/\Gamma(\Upsilon \rightarrow ggg)$ [5]. The calculated partial decay rates and branching fractions for $1P$ and $2P$ states of the bottomonium are compared with available experimental data in Table XI. There we give both PDG [22] averages and very recent CLEO [32] data. We see that our predictions for the branching fractions for radiative transitions of $\chi_b(nP)$ to

$\Upsilon(n'S)$ states are in good agreement with experiment. The only discrepancy (of 2.5σ) is the CLEO value for $\mathcal{B}(\chi_{b1}(2P) \rightarrow \Upsilon(2S) + \gamma)$ transition which is approximately two times larger than our model prediction and PDG value. The CLEO Collaboration [32] measured also two photon decays of $\Upsilon(3S)$ via $\chi_b(1P_J)$ states. They report the branching fraction for $\Upsilon(3S) \rightarrow \chi_b(1P_J) + \gamma \rightarrow \Upsilon(1S) + \gamma\gamma$ transitions summed over all the J states:

$$\mathcal{B}(\Upsilon(3S) \rightarrow \Upsilon(1S) + \gamma\gamma) = (2.14 \pm 0.22 \pm 0.21) \times 10^{-3}. \quad (68)$$

Using our model results in Tables IX–XI for corresponding decay rates, we get

$$\begin{aligned} \mathcal{B}(\Upsilon(3S) \rightarrow \chi_{b0}(1P) + \gamma \rightarrow \Upsilon(1S) + \gamma\gamma) &= 1.4 \times 10^{-5}, \\ \mathcal{B}(\Upsilon(3S) \rightarrow \chi_{b1}(1P) + \gamma \rightarrow \Upsilon(1S) + \gamma\gamma) &= 9.97 \times 10^{-4}, \\ \mathcal{B}(\Upsilon(3S) \rightarrow \chi_{12}(2P) + \gamma \rightarrow \Upsilon(1S) + \gamma\gamma) &= 9.96 \times 10^{-4}, \end{aligned}$$

and the sum over all the J states is equal to

$$\mathcal{B}(\Upsilon(3S) \rightarrow \Upsilon(1S) + \gamma\gamma) = 2.04 \times 10^{-3}$$

in accord with CLEO data (68).

The CLEO Collaboration [32] presented recently the first evidence for the production of the triplet $\Upsilon(1D)$ states in the four photon transitions $3S \rightarrow 2P + \gamma \rightarrow 1D + \gamma\gamma \rightarrow 1P + \gamma\gamma\gamma \rightarrow 1S + \gamma\gamma\gamma\gamma \rightarrow e^+e^- + \gamma\gamma\gamma\gamma$. The measured product branching fraction for these five decays is equal to $(3.3 \pm 0.6 \pm 0.5) \times 10^{-5}$. In Table XII we give the theoretical predictions for the branching fractions of such four photon decays in our model and in the recent quark model analysis of Godfrey and Rosner [6]. In general, both theoretical predictions are consistent. In the analysis of Ref. [6], the dominant decay is $3^3S_1 \rightarrow 2^3P_1 + \gamma \rightarrow 1^3D_2 + \gamma\gamma \rightarrow 1^3P_1 + \gamma\gamma\gamma \rightarrow 1^3S_1 + \gamma\gamma\gamma\gamma \rightarrow e^+e^- + \gamma\gamma\gamma\gamma$, while in our model the above and $3^3S_1 \rightarrow 2^3P_2 + \gamma \rightarrow 1^3D_3 + \gamma\gamma \rightarrow 1^3P_2 + \gamma\gamma\gamma \rightarrow 1^3S_1 + \gamma\gamma\gamma\gamma \rightarrow e^+e^- + \gamma\gamma\gamma\gamma$ transitions have almost the same rate and dominate. In the last line we give the sum of all these decay channels. Both theoretical predictions agree with CLEO measurement.

An important problem of quarkonium physics is the search for bottomonium spin singlet states $\eta_b(n^1S_0)$ and $h_b(n^1P_1)$. In the previous section we discussed the possibilities of finding η_b in radiative M1 decays. From Table XI we see that these two states can be discovered simultaneously. Indeed the radiative decay $h_b(1^1P_1) \rightarrow \eta_b(1^1S_0) + \gamma$ with the photon energy of 480 MeV is the main decay channel of h_b (the branching fraction of this decay exceeds 50%). Thus production of a few h_b states, e.g., through $\Upsilon''(3S) \rightarrow h_b(1^1P_1)\pi\pi$ or $\Upsilon''(3S) \rightarrow h_b(1^1P_1)\pi$ decays, which branching fractions are predicted to be about 0.1–1% [48], will give a good possibility of finding η_b .

In Tables XIII and XIV we compare our results for the E1 radiative decay rates of the B_c meson with other quark model predictions [33, 34, 35]. Comparison of the calculations using relativistic Γ and nonrelativistic Γ^{NR} formulae for decay rates shows that relativistic corrections do not exceed 20% in B_c meson E1 decays. Most of the theoretical predictions for E1 transitions between P and S states of B_c mesons given in Table XIII are compatible with each other. The largest differences occur for decays involving $P1$ and $P1'$ states which are the mixtures of spin singlet and spin triplet states (24) due to different mixing angles used by the authors. Note that for such transitions there are additional relativistic spin-flip contributions to decay rates (58) proportional to $\chi(J', L', J, L)$ (57) which are specific only for B_c mesons. In general, our predictions are closer to the ones of Ref. [34].

In Table XIV we present the E1 radiative decay rates of B_c mesons where either the initial or final state is a D wave state. Here we find rather large variations in theoretical

TABLE XI: Partial decay rates and branching fractions for $1P$ and $2P$ states of bottomonium.

Level	Decay	Γ (keV)	\mathcal{B} (%)	\mathcal{B}^{exp} (%)	
				PDG [22]	CLEO [32]
1^3P_0	gg	653	95.6		
	$1^3S_1 + \gamma$	29.9	4.4	< 6	
1^3P_1	$q\bar{q} + g$	57	60.9		
	$1^3S_1 + \gamma$	36.6	39.1	35 ± 8	
1^3P_2	gg	109	73		
	$1^3S_1 + \gamma$	40.2	27	22 ± 4	
1^1P_1	ggg	36	40.1		
	$gg + \gamma$	1.2	1.3		
	$1^1S_0 + \gamma$	52.6	58.6		
2^3P_0	gg	431	95.8		
	$2^3S_1 + \gamma$	11.0	2.4	4.6 ± 2.1	$2.59 \pm 0.92 \pm 0.51$
	$1^3S_1 + \gamma$	6.8	1.5	0.9 ± 0.6	< 1.44
	$1^3D_1 + \gamma$	1.17	0.3		
2^3P_1	$q\bar{q} + g$	50	67.2		
	$2^3S_1 + \gamma$	14.7	19.8	21 ± 4	$41.5 \pm 1.2 \pm 5.9$
	$1^3S_1 + \gamma$	7.5	10.0	8.5 ± 1.3	$11.6 \pm 0.4 \pm 0.9$
	$1^3D_1 + \gamma$	0.6	0.8		
	$1^3D_2 + \gamma$	1.6	2.2		
2^3P_2	gg	76	73.4		
	$2^3S_1 + \gamma$	16.7	16.1	16.2 ± 2.4	$19.3 \pm 1.1 \pm 3.1$
	$1^3S_1 + \gamma$	8.0	7.7	7.1 ± 1.0	$7.0 \pm 0.4 \pm 0.8$
	$1^3D_1 + \gamma$	0.04	0.03		
	$1^3D_2 + \gamma$	0.5	0.5		
	$1^3D_3 + \gamma$	2.4	2.3		
2^1P_1	ggg	31.5	47.9		
	$gg + \gamma$	1.1	1.7		
	$2^1S_0 + \gamma$	21.4	32.5		
	$1^1S_0 + \gamma$	9.4	14.3		
	$1^1D_2 + \gamma$	2.4	3.6		

predictions. The main reason of these distinctions is the difference in values of D state masses, which for some states reaches 70 MeV (see Table III). Since $2P$ and $1D$ states of the B_c are rather close, such a difference significantly influences the energy of the emitted photon and thus the decay rates. For decays involving the mixed spin singlet and spin triplet states $P1$, $P1'$ (24) and $D2$, $D2'$ (25) the additional relativistic spin-flip contributions (58) are important, especially for transitions where both initial and final states are mixed states.

TABLE XII: Predicted branching fractions of four photon decays of $\Upsilon(3S)$ involving $1D$ states corresponding to $3S \rightarrow 2P + \gamma \rightarrow 1D + \gamma\gamma \rightarrow 1P + \gamma\gamma\gamma \rightarrow 1S + \gamma\gamma\gamma\gamma \rightarrow e^+e^- + \gamma\gamma\gamma\gamma$ transition. The last line gives the sum of all decay channels.

2^3P_J state	1^3D_J state	1^3P_J state	\mathcal{B}^{our} ($\times 10^{-6}$)	\mathcal{B} [6] ($\times 10^{-6}$)
2^3P_2	1^3D_3	1^3P_2	15.2	7.8
		1^3P_2	0.7	0.3
	1^3D_1	1^3P_1	3.9	2.7
		1^3P_2	0.0	0.0
		1^3P_1	0.1	0.1
		1^3P_0	0.0	0.0
2^3P_1	1^3D_2	1^3P_2	2.9	2.5
		1^3P_1	15.5	20.1
	1^3D_1	1^3P_2	0.1	0.1
		1^3P_1	2.4	3.3
		1^3P_0	0.5	0.4
2^3P_0	1^3D_1	1^3P_2	0.0	0.0
		1^3P_1	0.5	0.3
		1^3P_0	0.0	0.0
all	all	all	41.8	37.6

VIII. CONCLUSIONS

In this paper the mass spectra and radiative M1 and E1 decay rates of charmonium, bottomonium and B_c mesons were calculated in the relativistic quark model based on the quasipotential approach in quantum field theory. Special attention was devoted to the role of the relativistic effects in these processes. Since both quarks in the considered mesons are heavy, the v/c expansion was applied. In the mass spectra calculations retardation as well as one-loop radiative corrections were taken into account. We also included the one-loop correction due to the finite charm quark mass to the bottomonium mass spectrum. It was found that this correction is rather small [31] and its inclusion allows one to obtain an even better fit of the bottomonium excited states with the slightly shifted value of QCD parameter Λ . The calculated mass spectra of charmonium and bottomonium agree with the experimental data within a few MeV. Comparison of our results for the B_c meson mass spectrum with previous calculations showed that different predictions for ground state and low excitations agree within 30 MeV.

The pseudoscalar and vector decay constants of B_c meson were calculated using the relativistic wave functions obtained during the mass spectrum calculations. It was found that relativistic effects reduce these constants by approximately 20% and produce the splitting between them of about 70 MeV.

It was shown that relativistic effects play a significant role in radiative decays of mesons. Their form strongly depends on the Lorentz structure of the quark-antiquark interaction. The most sensitive are radiative M1 decays, where even for allowed transitions they significantly influence predictions for the rates. An important example is the $J/\Psi \rightarrow \eta_c\gamma$

TABLE XIII: Radiative E1 transition rates of the B_c meson.

Decay	ω MeV	Γ^{NR} keV	Γ^V keV	Γ^S keV	Γ keV	Γ [33] keV	Γ [34] keV	Γ [35] keV
$1^3P_0 \rightarrow 1^3S_1\gamma$	355	75.5	74.1	81.3	67.2	79.2	65.3	74.2
$1P1 \rightarrow 1^3S_1\gamma$	389	87.1	82.9	87.1	78.9	99.5	77.8	75.8
$1P1' \rightarrow 1^3S_1\gamma$	405	13.7	12.6	11.6	13.6	0.1	8.1	26.2
$1^3P_2 \rightarrow 1^3S_1\gamma$	416	122	105	102	107	112.6	102.9	126
$1P1 \rightarrow 1^1S_0\gamma$	447	18.4	16.3	14.4	18.4	0.0	11.6	32.5
$1P1' \rightarrow 1^1S_0\gamma$	463	147	134	136	132	56.4	131.1	128
$2^3S_1 \rightarrow 1^3P_0\gamma$	181	5.53	4.36	5.00	3.78	7.8	7.7	9.6
$2^3S_1 \rightarrow 1P1\gamma$	146	7.65	5.98	6.98	5.05	14.5	12.8	13.3
$2^3S_1 \rightarrow 1P1'\gamma$	130	0.74	0.62	0.61	0.63	0.0	1.0	2.5
$2^3S_1 \rightarrow 1^3P_2\gamma$	118	7.59	5.99	6.86	5.18	17.7	14.8	14.5
$2^1S_0 \rightarrow 1P1\gamma$	101	1.05	0.94	0.86	1.02	0.0	1.9	6.4
$2^1S_0 \rightarrow 1P1'\gamma$	84	4.40	3.77	3.82	3.72	5.2	15.9	13.1
$2^3P_0 \rightarrow 2^3S_1\gamma$	207	34.0	28.8	28.4	29.2	41.2	25.5	
$2P1 \rightarrow 2^3S_1\gamma$	241	45.3	37.6	37.3	37.9	54.3	32.1	
$2P1' \rightarrow 2^3S_1\gamma$	259	10.4	8.45	7.86	9.07	5.4	5.9	
$2^3P_2 \rightarrow 2^3S_1\gamma$	270	75.3	58.9	60.6	57.3	73.8	49.4	
$2P1 \rightarrow 2^1S_0\gamma$	285	13.8	11.1	10.5	11.7		8.1	
$2P1' \rightarrow 2^1S_0\gamma$	303	90.5	73.2	73.8	72.5		58.0	

transition, which is overestimated by a factor of more than two if the nonrelativistic approximation is used. It is argued that the inclusion of relativistic corrections for a pure scalar or vector confining potential is not enough to bring theoretical predictions in accord with experiment. Only for the specific mixture of these potentials (9) with the mixing coefficient $\varepsilon = -1$, the agreement can be obtained. For other decay rates this mixing of scalar and vector potentials also gives the best results. The hindered M1 transition rates are dominated by relativistic contributions and are significantly enhanced by them. The comparison of the allowed and hindered M1 rates in bottomonium shows that the latter provide better opportunity for the search of the missing pseudoscalar η_b state of the bottomonium.

The analysis of radiative E1 transitions showed that the form of relativistic corrections is less dependent on the Lorentz structure of the quark potential than in the case of M1 transitions. However, for some decays, e.g., $\Psi' \rightarrow \chi_{cJ}\gamma$, the consideration of the mixed (9) vector and scalar potentials (with the same value of $\varepsilon = -1$) is important for bringing decay rates in accord with experimental data. In general, all our predictions for radiative decay rates and branching fractions of charmonium and bottomonium agree with measured values. In the case of the B_c meson radiative E1 decays an important additional relativistic correction to decay rates which causes the flip of the quark spin was found. This contribution (57) to the radiative E1 decay rate (58) is specific only for transitions involving mixed states $nP1$, $nP1'$ (24) or $nD2$, $nD2'$ (25) of B_c and is caused by the difference of the c and b quark masses. Finally, a comparison of various quark model predictions for the radiative M1 and E1 decay rates of B_c has been performed. These radiative transitions along with pionic ones

TABLE XIV: Radiative E1 transition rates of the B_c meson involving D states.

Decay	ω MeV	Γ^{NR} keV	Γ^{V} keV	Γ^{S} keV	Γ keV	Γ [33] keV	Γ [34] keV
$2^3P_2 \rightarrow 1^3D_1\gamma$	84	0.035	0.031	0.027	0.035	0.2	0.1
$2^3P_2 \rightarrow 1D2\gamma$	79	0.285	0.245	0.222	0.269	3.2	1.5
$2^3P_2 \rightarrow 1D2'\gamma$	77	0.139	0.114	0.116	0.113		0.5
$2^3P_2 \rightarrow 1^3D_3\gamma$	75	2.08	1.64	1.69	1.59	17.8	10.9
$2^3P_0 \rightarrow 1^3D_1\gamma$	19	0.041	0.034	0.033	0.036	6.9	3.2
$2P1 \rightarrow 1^3D_1\gamma$	54	0.204	0.174	0.165	0.184	0.3	1.6
$2P1' \rightarrow 1^3D_1\gamma$	73	0.070	0.062	0.052	0.073	0.4	0.3
$2P1 \rightarrow 1D2\gamma$	49	0.517	0.420	0.422	0.418	9.8	3.9
$2P1 \rightarrow 1D2'\gamma$	47	0.023	0.019	0.018	0.021		1.2
$2P1' \rightarrow 1D2\gamma$	68	0.172	0.142	0.135	0.149	11.5	2.5
$2P1' \rightarrow 1D2'\gamma$	66	1.49	1.20	1.20	1.20		3.5
$1^3D_1 \rightarrow 1^3P_0\gamma$	365	133	119	110	128	88.6	79.7
$1^3D_1 \rightarrow 1P1\gamma$	331	65.3	63.7	54.2	73.8	49.3	39.2
$1^3D_1 \rightarrow 1P1'\gamma$	315	7.81	6.91	6.20	7.66	0.0	3.3
$1^3D_1 \rightarrow 1^3P_2\gamma$	303	3.82	4.27	3.17	5.52	2.7	2.2
$1D2 \rightarrow 1P1\gamma$	335	139	112	113	112	88.8	44.6
$1D2 \rightarrow 1P1'\gamma$	319	14.9	13.4	12.7	14.1	0.1	18.4
$1D2' \rightarrow 1P1\gamma$	338	7.10	6.70	6.17	7.25		25.0
$1D2' \rightarrow 1P1'\gamma$	321	143	116	117	116	92.5	46.0
$1D2 \rightarrow 1^3P_2\gamma$	308	23.6	23.4	19.7	27.5	24.7	12.2
$1D2' \rightarrow 1^3P_2\gamma$	310	12.6	11.4	10.1	12.8		6.8
$1^3D_3 \rightarrow 1^3P_2\gamma$	312	149	112	122	102	98.7	76.9

are the main decay channels of the low lying excitations in the B_c meson.

Acknowledgments

The authors express their gratitude to A. Martin, M. Müller-Preussker and V. Savrin for support and discussions. We are grateful to J. L. Rosner for stimulating correspondence and quoting some of our preliminary results on bottomonium radiative transitions in Ref. [4]. Two of us (R.N.F and V.O.G.) were supported in part by the *Deutsche Forschungsgemeinschaft* under contract Eb 139/2-1, *Russian Foundation for Basic Research* under Grant No. 00-02-17768 and *Russian Ministry of Education* under Grant No. E00-3.3-45.

-
- [1] E. J. Eichten, K. Lane and C. Quigg, Phys. Rev. Lett. **89**, 162002 (2002).
 - [2] M. Suzuki, Phys. Rev. D **66**, 037503 (2002).
 - [3] Y.-P. Kuang, Phys. Rev. D **65**, 094024 (2002).

- [4] S. Godfrey and J. L. Rosner, Phys. Rev. D **64**, 074011 (2001); **65**, 039901(E) (2002).
- [5] S. Godfrey and J. L. Rosner, Phys. Rev. D **66**, 014012 (2002).
- [6] S. Godfrey and J. L. Rosner, Phys. Rev. D **64**, 097501 (2001).
- [7] CDF Collaboration, F. Abe *et al.*, Phys. Rev. D **58**, 112004 (1998).
- [8] A. A. Logunov and A. N. Tavkhelidze, Nuovo Cimento **29**, 380 (1963).
- [9] A. P. Martynenko and R. N. Faustov, Theor. Math. Phys. **64**, 765 (1985) [Teor. Mat. Fiz. **64**, 179 (1985)].
- [10] V. O. Galkin, A. Yu. Mishurov and R. N. Faustov, Yad. Fiz. **55**, 2175 (1992) [Sov. J. Nucl. Phys. **55**, 1207 (1992)].
- [11] D. Ebert, R. N. Faustov and V. O. Galkin, Phys. Rev. D **62**, 034014 (2000).
- [12] E. Eichten and F. Feinberg, Phys. Rev. D **23**, 2724 (1981).
- [13] D. Ebert, V. O. Galkin and R. N. Faustov, Phys. Rev. D **57**, 5663 (1998); **59**, 019902(E) (1999).
- [14] V. O. Galkin and R. N. Faustov, Yad. Fiz. **44**, 1575 (1986) [Sov. J. Nucl. Phys. **44**, 1023 (1986)]; D. Ebert, R. N. Faustov and V. O. Galkin, Phys. Lett. B **537**, 241 (2002).
- [15] R. N. Faustov and V. O. Galkin, Z. Phys. C **66**, 119 (1995).
- [16] N. Brambilla, P. Consoli and G. M. Prospero, Phys. Rev. D **50**, 5878 (1994).
- [17] S. N. Gupta and S. F. Radford, Phys. Rev. D **24**, 2309 (1981); *ibid.* **25**, 3430 (1982); S. N. Gupta, S. F. Radford and W. W. Repko, Phys. Rev. D **26**, 3305 (1982).
- [18] J. Pantaleone, S.-H. H. Tye and Y. J. Ng, Phys. Rev. D **33**, 777 (1986).
- [19] W. Buchmüller, Phys. Lett. B **112**, 479 (1982).
- [20] N. Brambilla and A. Vairo, Phys. Rev. D **55**, 3974 (1997).
- [21] H. J. Schnitzer, Phys. Rev. Lett. **35**, 1540 (1975); W. Lucha, F. F. Schöberl and D. Gromes, Phys. Rep. **200**, 127 (1991); V. D. Mur, V. S. Popov, Yu. A. Simonov and V. P. Yurov, Zh. Eksp. Teor. Fiz. **78**, 1 (1994) [J. Exp. Theor. Phys. **78**, 1 (1994)]; A. Yu. Dubin, A. B. Kaidalov and Yu. A. Simonov, Phys. Lett. B **323**, 41 (1994); Yu. A. Simonov, Phys. Usp. **39**, 313 (1996).
- [22] Particle Data Group, K. Hagiwara *et al.*, Phys. Rev. D **66**, 010001 (2002).
- [23] Belle Collaboration, S.-K. Choi *et al.*, Phys. Rev. Lett. **89**, 102001 (2002).
- [24] C. Edwards *et al.*, Phys. Rev. Lett. **48**, 70 (1982).
- [25] T. A. Armstrong *et al.*, Phys. Rev. Lett. **69**, 2337 (1992).
- [26] E705 Collaboration, L. Antoniazzi *et al.*, Phys. Rev. D **50**, 4258 (1994).
- [27] A. H. Hoang and A. V. Manohar, Phys. Lett. B **491**, 101 (2000).
- [28] A. H. Hoang, hep-ph/0008102, hep-ph/0204299.
- [29] M. Melles, Phys. Rev. D **62**, 074019 (2000).
- [30] N. Brambilla, Y. Sumino and A. Vairo, Phys. Rev. D **65**, 034001 (2002).
- [31] D. Ebert, R. N. Faustov and V. O. Galkin, Phys. Rev. D **66**, 037501 (2002).
- [32] CLEO Collaboration, S. E. Csorna *et al.*, hep-ex/0207060; D. Cinabro *et al.*, hep-ex/0207062.
- [33] E. J. Eichten and C. Quigg, Phys. Rev. D **49**, 5845 (1994).
- [34] S. S. Gershtein, V. V. Kiselev, A. K. Likhoded, and A. V. Tkabladze, Phys. Rev. D **51**, 3613 (1995).
- [35] L. P. Fulcher, Phys. Rev. D **60**, 074006 (1999).
- [36] S. Nussinov and M. A. Lampert, Phys. Rep. **362**, 193 (2002).
- [37] W. Kwong and J. L. Rosner, Phys. Rev. D **44**, 212 (1991).
- [38] N. Brambilla and A. Vairo, Phys. Rev. D **62**, 094019 (2000).
- [39] D. Ebert, R. N. Faustov and V. O. Galkin, Mod. Phys. Lett. A **17**, 803 (2002); V. O. Galkin,

- A. Yu. Mishurov and R. N. Faustov, *Yad. Fiz.* **53**, 1676 (1991) [*Sov. J. Nucl. Phys.* **53**, 1026 (1991)].
- [40] B. D. Jones and R. M. Woloshyn, *Phys. Rev. D* **60**, 014502 (1999).
- [41] R. N. Faustov, *Ann. Phys. (N. Y.)* **78**, 176 (1973); *Nuovo Cimento A* **69**, 37 (1970).
- [42] CLEO Collaboration, A. H. Mahmood *et al.*, hep-ex/0207057.
- [43] V. O. Galkin, A. Yu. Mishurov and R. N. Faustov, *Yad. Fiz.* **51**, 1101 (1990) [*Sov. J. Nucl. Phys.* **51**, 705 (1990)].
- [44] J. L. Rosner, *Phys. Rev. D* **64**, 094002 (2001).
- [45] V. A. Novikov *et al.*, *Phys. Rep.* **41**, 1 (1978); R. Barbieri, R. Gatto and R. Kogerler, *Phys. Lett. B* **60**, 183 (1976); R. Barbieri, M. Caffo, R. Gatto, and E. Remiddi, *Nucl. Phys. B* **192**, 61 (1981).
- [46] W. Kwong, P. B. Mackenzie, R. Rosenfeld, and J. L. Rosner, *Phys. Rev. D* **37**, 3210 (1988).
- [47] R. N. Faustov and V. O. Galkin, *Proceedings of the International Seminar "Quarks'88"*, Tbilisi, 17-21 May 1988 (World Scientific, Singapore, 1989), p. 624.
- [48] Y.-P. Kuang and T.-M. Yan, *Phys. Rev. D* **24**, 2874 (1981); M. Voloshin, *Yad. Fiz.* **43**, 1571 (1986) [*Sov. J. Nucl. Phys.* **43**, 1011 (1986)].